Applied Clay Science 216 (2022) 106331

Contents lists available at ScienceDirect

Applied Clay Science

journal homepage: www.elsevier.com/locate/clay

Impact of anoxic conditions, uranium(VI) and organic phosphate substrate on the biogeochemical potential of the indigenous bacterial community of bentonite

Cristina Povedano-Priego [a,*], Fadwa Jroundi [a], Margarita Lopez-Fernandez [b], Mar Morales-Hidalgo [a], Inés Martin-Sánchez [a], F. Javier Huertas [c], Mark Dopson [b], Mohamed L. Merroun [a]

[a] Department of Microbiology, Faculty of Sciences, University of Granada, Granada, Spain
[b] Centre for Ecology and Evolution in Microbial Model Systems (EEMiS), Linnaeus University, Kalmar, Sweden
[c] Instituto Andaluz de Ciencias de la Tierra, CSIC – University of Granada, Granada, Spain

ARTICLE INFO

Keywords:
Bacterial diversity
DGR
Radionuclides
G2P
Bioreduction
Immobilization

ABSTRACT

Uranium (U) is the most hazardous radionuclide in nuclear waste and its harmful effects depend on its mobility and bioavailability. Microorganisms can affect the speciation of radionuclides and their migration in Deep Geological Repositories (DGR) for high level radioactive waste (HLW) storage. Consequently, a better understanding of microbe-radionuclide interactions within a DGR concept is essential for a safe storage. With that in mind, bentonite microcosms amended with uranyl nitrate and glycerol-2-phosphate were incubated for six months under anoxic conditions. Post-incubation 16S rRNA gene sequencing revealed high microbial diversities including glycerol oxidizers such as *Clostridium* and *Desulfovibrio* and nitrate reducers (*Limnobacter* and *Brevundimonas*). In addition, uranium-reducing bacteria (*Desulfovibrio* and *Pseudomonas*) were highly enriched in glycerol-2-phosphate-uranium amended microcosms. These bacteria may contribute to uranium immobilization through enzymatic reduction and/or biomineralization. Scanning electron microscopy of colored spots on the surface of the bentonite in the microcosms indicated the probable formation of Mn(IV) oxides likely through the activity of Mn(II)-oxidizing microbes. This could affect the biogeochemical cycle of U(VI) by concentrating and immobilizing this element in the bentonites. Finally, X-ray diffraction determined a high structural stability of bentonites. The outputs of this study help to predict the impact of microbial activity (e.g. smectite alteration, metal corrosion, and radionuclides mobilization) on the long-term performance of a DGR and to develop appropriate waste treatments, remediation, and management strategies.

1. Introduction

The use of Deep Geological Repositories (DGRs) is the option accepted by many countries for the management of highly-radioactive waste (mainly spent fuel and waste material from reprocessing) (Grigoryan et al., 2018), although their construction is still in progress worldwide (Pedersen et al., 2017). The DGR concept involves a multi-barrier system comprising the storage of spent fuel in metal canisters (cast iron, stainless steel, or copper, depending on the strategy selected for each country), usually surrounded by a further engineered barrier consisting of a highly-compacted bentonite clay (Anderson et al., 2011; Bengtsson and Pedersen, 2017). Smectite rich bentonites are the most suitable backfill materials for DGRs since they possess a high swelling capacity, plasticity, low permeability, and high sorption ability for radionuclide retardation (Masurat et al., 2010; Missana et al., 2003). Bentonite from the "El Cortijo de Archidona" (Almeria, south-east Spain) deposit has been designated as the engineered barrier material for the planned DGR in Spain (Villar et al., 2006). A detailed mineralogical characterization was reported by Huertas et al. (2006).

Since microorganisms are ubiquitous in all environments, their influence on DGR safety has been studied extensively in several bentonites from different sites (Bengtsson and Pedersen, 2017; Leupin et al., 2017;

* Corresponding author at: Department of Microbiology, Faculty of Sciences, University of Granada, Campus Fuentenueva s/n, 18071 Granada, Spain.
E-mail addresses: ppriego@ugr.es, fadwa@ugr.es (C. Povedano-Priego), margaritalopez@ugr.es (M. Lopez-Fernandez), marmh@ugr.es (M. Morales-Hidalgo), inesms@ugr.es (I. Martin-Sánchez), javierhuertas@ugr.es (F.J. Huertas), mark.dopson@lnu.se (M. Dopson), merroun@ugr.es (M.L. Merroun).

https://doi.org/10.1016/j.clay.2021.106331
Received 15 June 2021; Received in revised form 30 October 2021; Accepted 2 November 2021
Available online 22 November 2021

Lopez-Fernandez et al., 2018; Pedersen et al., 2017; Smart et al., 2017). Microbial processes such as gas release, sulfide production and Fe(III) reduction could affect the integrity and safety of the radioactive waste repository through metal corrosion and bentonite alteration (Liu et al., 2017; Pentráková et al., 2013; Stone et al., 2016; Stroes-Gascoyne et al., 2010). Furthermore, microbial mechanisms (biosorption, intracellular accumulation, biomineralization, and bioreduction) can control the speciation and mobility of radionuclides in the case of canister failure (Lopez-Fernandez et al., 2018; Povedano-Priego et al., 2019). While microbes can affect uranium speciation, this radionuclide may in turn influence the bacterial community by enriching species with a high U-tolerance. For instance, the presence of U(VI) changes the indigenous bacterial community of soils/bentonites (Lopez-Fernandez et al., 2018; Newsome et al., 2015; Povedano-Priego et al., 2019). Hence, it is relevant to consider both the bacterial diversity and the uranium speciation in case uranium is released in the DGR.

The impact of bentonite microbial populations on uranium mobility and its effects on bacterial diversity under aerobic conditions revealed the enrichment of e.g., *Bacillus* spp. involved in biomineralization of U-phosphate mineral phases (Lopez-Fernandez et al., 2018; Povedano-Priego et al., 2019). However, uranium biomineralization is greatly heightened by the presence of organophosphates (e.g. glycerol-2-phosphate [G2P]) (Martinez et al., 2014). Thus, Povedano-Priego et al. (2019) focused on the combined effect of G2P (the substrate for phosphatases) and uranium under aerobic conditions, observing the release of inorganic phosphates leading to uranium precipitation (biomineralization). In the DGR concept, oxygen introduced during construction and canister emplacement will likely be consumed within two years via microbial activities, corrosion processes, or mineral oxidation (King et al., 2017; Payer et al., 2019). Therefore, due to the anoxic conditions present in the DGR for thousands of years, bentonite microbial diversity needs to be addressed under anaerobic conditions.

Radionuclide-microorganism interaction mechanisms can occur under anaerobic and reducing environments, for instance bioreduction of U(VI) to less soluble U(IV) (Newsome et al., 2014a). Under these conditions, the microbial community may include sulfate-reducing bacteria (SRB; e.g., *Desulfovibrio*), iron-reducing bacteria (IRB; e.g., *Geobacter*), denitrifiers (e.g., *Pseudomonas*), and spore-forming species such as *Clostridium* (Chabalala and Chirwa, 2010; Cologgi et al., 2011; Gao and Francis, 2008; Stylo et al., 2015; Vecchia et al., 2010). The dominant product of microbial uranium reduction is often reported to be uraninite [UO_2] although other minerals have been identified recently as bioreduced uranium, including ningyoite [$CaU(PO_4)_2$] produced by *Thermoterrabacterium ferrireducens* and *Desulfotomaculum reducens* along with monomeric U(IV) by *Shewanella oneidensis* (Alessi et al., 2012; Bernier-Latmani et al., 2010; Newsome et al., 2014a). However, the bioreduced U(IV) can be reoxidized to U(VI), especially in the presence of nitrate and/or e.g., Fe(III) (Xu et al., 2017). In the DGR, nitrate can be introduced during the construction process, on rock surfaces, and in the groundwater (Kutvonen et al., 2015). Therefore, it is interesting to also consider the impact of nitrates on the biogeochemical cycle of U under DGR relevant conditions.

This study investigated the effects of uranyl nitrate and G2P on: 1) the mineralogy and structure of bentonites, and 2) the composition of the bacterial community of these clays. The study helps to predict the impact of microbial processes (e.g. smectite alteration by Fe(III)-reducing activity, metal corrosion through the sulfide production by SRB, and the immobilization of U via different mechanisms) on the long-term performance of the DGR once in situ anaerobic conditions are established.

2. Materials and methods

2.1. Treatments and incubation of bentonite microcosms

Bentonite from El Cortijo de Archidona (Almeria, Spain) was collected under aseptic conditions at a depth of 0.8 m using a manual auger previously cleaned with ethanol. Bentonite was stored in sterile containers, and kept at 4 °C in the laboratory (Supplementary Fig. S1). The sample collection was performed in January 2016. This bentonite presents a high mineralogical purity with 92% of dioctahedral smectite, 3% of plagioclases, and 2% of cristobalite and quartz (Villar et al., 2006). Rozalen et al. (2008) after transmission electron microscopy analysis classified this dioctahedral smectite as montmorillonite. (Hereinafter we use the term bentonite for the clay-type rock and smectite for the clay minerals). The bentonite was used for the establishment of anaerobic microcosms: 40 g of ground bentonite in sterile Petri dishes (Supplementary Fig. S1). Bentonite microcosms were treated with different solutions: 1) 1.26 mM uranyl nitrate to investigate the effect of uranium after incubation (U samples); 2) 10 mM glycerol-2-phosphate (G2P) and 1.26 mM uranyl nitrate to determine the impact of uranium in the presence of an organic phosphate source (GU samples); 3) 10 mM G2P (G samples); 4) 2.71 mM sodium nitrate (N samples) as a control of the uranyl nitrate treatment; 5) 10 mM G2P and 2.71 mM sodium nitrate (GN samples); and 6) distilled water (H samples) as a control for G and N samples (Supplementary Fig. S1). G2P was added as a carbon and phosphate source to stimulate the growth of the indigenous bacteria in the bentonite. In the DGR concept, G2P is usually present as cell wall compounds of bacteria and fungi (Martinez et al., 2014) and in addition, it may derive from the hydrolysis of teichoic acids from Gram-positive bacteria (Weidenmaier and Peschel, 2008). All the working solutions were sterilized by filtration through 0.22 μm pore-size nitrocellulose filters and homogenously added to bentonite until complete saturation of the clays in the plates (Supplementary Fig. S1). Treatments were carried out in triplicate. A total of 18 individual microcosms were incubated under anaerobic conditions for six months in darkness at room temperature (Supplementary Fig. S2). To establish the anaerobic conditions, the microcosms-containing plates were placed in an anaerobic jar (BBL™ GasPak™ Anaerobic Systems) with anaerobiosis generator sacks (AnaeroGen™, Thermo Scientific; Supplementary Fig. S2B) establishing a CO_2 atmosphere. To allow the diffusion of the anaerobic atmosphere created inside the anaerobic jar, plates were closed with their cover without extra sealing with Parafilm (M). Although bentonite in these microcosms was not compacted, bentonite would be confined in the DGR resulting in a decrease of the microbial growth. After incubation, samples were stored at −20 °C until further use.

2.2. Chemical and mineralogical characterization of anaerobic microcosms

The pH of each sample was measured in triplicate according to the method of Stone et al. (2016): one gram of bentonite was mixed with 15 mL $CaCl_2$ (0.01 M) solution at 1:15 bentonite:solvent ratio. A Crison pH-meter (MicropH, 2002) was used calibrated against pH 4.00 and 7.02 commercial reference solutions (± 0.02 pH units of reported accuracy).

Mineralogy of the bentonite after six-month incubation was determined by X-ray diffraction (XRD) analyses using a PANalytical X'Pert Pro diffractometer equipped with an X'Celerator solid-state detector (0.25° divergence slit, Ni filter). XRD patterns were recorded using random oriented mounts with CuKα radiation (λ = 1.5405 Å), operated at 45 kV and 40 mA, scanned from 4 to 70°2θ. Bentonite from microcosms was sampled with a spatula, without removing the brown spots at the surface. These samples were desiccated at 50 °C and then ground to obtain a fine powder. The limited amount of bentonite available for the analysis, sprinkled over a zero-background silicon sample holder, may produce preferential orientation of some crystals and distortion of relative intensities in XRD patterns with respect to ideal conditions for random powder. Mineral phases were identified by comparison with JCPDS powder spectra (Joint Committee on Powder Diffraction Standards).

2.3. Microscopic characterization of the anaerobic microcosms

High-Angle Annular Dark Field Scanning Transmission Electron Microscope [(HAADF-STEM) FEI TITAN G2 80–30] and Energy Dispersive X-ray Spectroscopy (EDX) microanalyses were used to ascertain the microstructural characteristics and elemental composition of the bentonite in the differently-treated microcosms after six months of incubation. The analyses were performed at an acceleration voltage of 300 kV. Microcosm samples were mixed in ethanol and dispersed by sonication, then they were deposited on carbon-coated copper grids as described in Povedano-Priego et al. (2019).

After six months of anaerobic incubation, colored spots on the surface of the microcosms were analyzed using Variable Pressure Field Emission Scanning Electron Microscopy [(VP-FESEM), *ZeissSupra 40VP*] equipped with SE (InLens) and BSE detectors to provide morphological and chemical images, respectively. For elemental analysis, the EDX detector used a 50 mm^2 silicon drift detector XMAX enabling detection of elements with Z4≥(Be) and high-count rates.

2.4. Bacterial diversity analyses of the treated anaerobic microcosms

2.4.1. Total DNA isolation from anaerobic microcosms

DNA was extracted from the anaerobic microcosms (H, N, U, G, GN, and GU; total 18 microcosms) after six months of incubation. From each microcosm, 0.3 g of moist bentonite was added in a 1.5 mL tube containing glass beads (~0.3 g) of different diameters, then a 0.12 M Na_2HPO_4 solution, and a lysis buffer were added. Afterwards, a phenol: chloroform method described in detail by Povedano-Priego et al. (2021) was followed to obtain the total DNA from bentonite samples. The concentration of the extracted total DNA was measured on a Qubit 3.0 Fluorometer (Life Technology) and stored at −20 °C.

2.4.2. Amplification and sequencing of the extracted DNA

The V3–V4 region of the 16S rRNA gene from each microcosm was amplified by a two-step PCR using bacterial primers 341F (5'-CCTACGGGNGGCWGCAG- 3′) and 805R (5'-GACTACHVGGGTATC-TAATCC- 3′) (Herlemann et al., 2011) following the PCR protocol described in Hugerth et al. (2014). 16S rRNA gene amplicon libraries were sequenced at Science for Life Laboratory (Sweden) on the Illumina MiSeq platform (2 × 300 bp pair-end reads). While the microcosms were prepared in triplicates, DNA sequencing failed in one of each sample (poor sequencing quality) resulting in duplicate data reported for microbial diversity and community analyses.

All raw sequences for this study are available in the sequence read archive (SRA) at the NCBI database under the accession number PRJNA669434.

2.4.3. Bioinformatics and statistical analyses of the bacterial community in the bentonite microcosms

Sample-specific barcodes were used for demultiplexing and separation of the PCR reads (Hugerth et al., 2014). Operational Taxonomic Units (OTUs) were obtained at 97% similarity threshold, following a quality control and combination and clustering of the paired-end reads. OTUs were identified using UCLUST (Edgar, 2010) and classified using the SILVA 132 database (Quast et al., 2013). Finally, the resulting annotated OTUs were analyzed in Explicet 2.10.5 (Robertson et al., 2013) and bar graphs of relative abundance were constructed representing averages of biological replicates as this has been found to be more accurate than rarefying (McMurdie and Holmes, 2013). Specific differences in the bacterial diversity were further visualized in a heatmap using R software ('heatmap.2' function, 'gplots' v.3.0.1.1 package) and including only taxa with ≥1% relative abundance in at least one replicate (Warnes et al., 2019). Microbial community composition at the OTU level was analyzed using weighted UniFrac distance (QIIME) and the output was visualized with Principal Coordinate Analysis (PCoA) using PAST3 v.3.18 software (Hammer et al., 2001). After normalization of all counts per taxa, significant differences in relative abundance ($p < 0.05$) between the different treatments were estimated using a one-way Analysis of Variance (ANOVA) test. In addition, a one-way ANOVA Tukey posthoc test was used to determine the significant differences ($p < 0.05$) in the relative abundance of the taxa between pairs of the six treatments for the total community. Moreover, linear discriminate analysis effect size (LEfSe) was performed to identify taxa that differed significantly among the bentonite microcosms by the non-parametric Kruskal-Wallis test, followed by the pairwise Wilcoxon rank-sum test and linear discriminant analysis (LDA) to measure the effect size and biological consistency within groups. Data output are taxa with LDA ≥2 and $p < 0.05$ (Segata et al., 2012).

3. Results and discussion

3.1. Changes in the chemistry and mineralogy of the treated anaerobic microcosms

Chemical analyses of bentonite samples prior to incubation are detailed in Povedano-Priego et al. (2019). The measured pH values of the bentonite samples (time 0 and 6-month incubation) ranged between 7.53 and 10.02 (Supplementary Table S1). The pH values of the bentonites, except for the distilled water sample, were less alkaline in all treatments after six months of incubation in comparison with those of time zero. While after six months the distilled water microcosms were more alkaline (with a value of 10.02) compared to the other microcosms, no significant differences in pH were observed among the treated microcosms. The pH values in the anaerobic microcosms (pH 7.53–8.04) were similar to those of the microcosms incubated under aerobic conditions, which ranged from 7.9 to 8.18 (Povedano-Priego et al., 2019).

This pH decrease during incubation in experiments with bentonite from "El Cortijo de Archidona" was previously demonstrated in a lixiviation process (Díaz-Fernández, 2004). The drop in pH could be explained further by smectite protonation/deprotonation reactions under anaerobic conditions (Nessa et al., 2007), production of carbon dioxide, and formation of organic acids (butyrate and acetate) during bacterial fermentation (Luo et al., 2019). 16S rRNA gene sequences belonging to *Clostridium* (a fermenting bacterial genus) were found in all the samples, and this presence could contribute to the production of organic acids (e.g. formate, and acetate) (Biebl, 2001; Patil et al., 2016; Temudo et al., 2008).

The XRD semi-quantitative estimation of the bentonite mineralogical composition at time zero (T0) was: smectite (91%), quartz (4%), phyllosilicates (2%), and plagioclase (2%) (Povedano-Priego et al., 2019). Mineralogy of the microcosms was similar to raw bentonite (T0), within an error of 10%. XRD patterns revealed peaks of smectite as the dominant mineral phase with minority mineral phases such as quartz, mica, cristobalite, and plagioclase (Fig. 1). Some samples exhibited isolated reflections (* in Fig. 1) that were associated to carbonates or nitrates (sample N), but the diffraction patterns were incomplete. Carbonates likely precipitated due to alkaline pH and CO_2 atmosphere used to produce the anaerobic conditions. The mineralogy remained similar in all the anaerobic microcosms compared to the time zero samples, indicating the stability of bentonite during the incubation period and no illitization process was observed. This outcome is highly reassuring for the safety of DGRs since smectite-to-illite transformation could result in a decrease in swelling ability and adsorption capabilities (Dong, 2012). It is critical that smectites remain chemically stable to avoid changes in the bentonite that could lead to severe consequences for the DGRs safety (Perdrial et al., 2009).

3.2. Microscopic characterization of bentonite minerals in anaerobic microcosms

3.2.1. HAADF-STEM analyses of bentonite

After six months of anaerobic incubation, STEM and EDX analyses

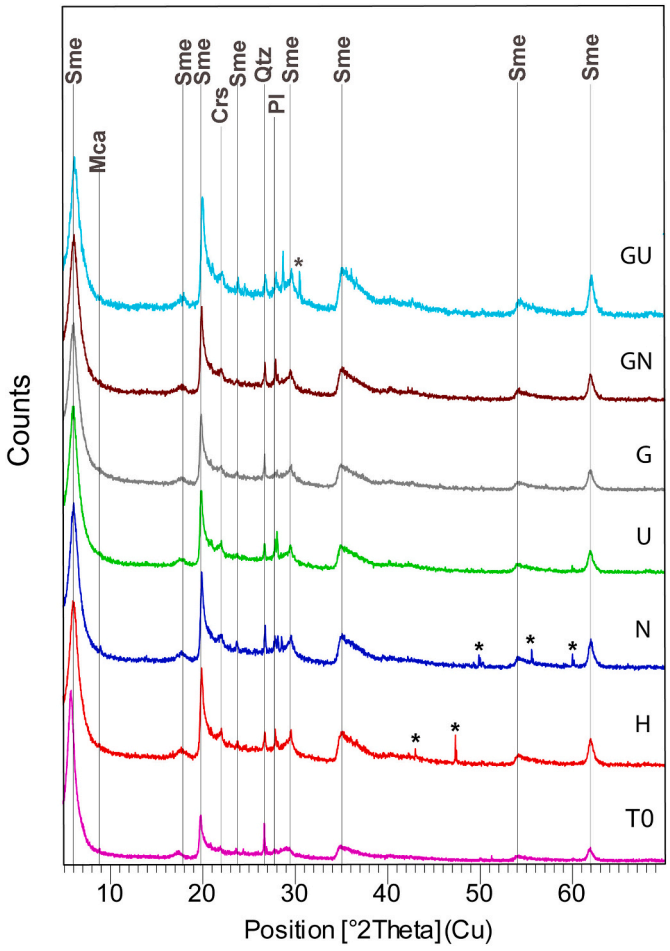

Fig. 1. X-ray Diffraction (XRD) patterns of bentonite microcosm samples treated with: distilled water (H), sodium nitrate (N), uranyl nitrate (U), glycerol-2-phosphate (G), glycerol-nitrate (GN), and glycerol-uranyl-nitrate (GU). T0 represents the untreated bentonite before incubation (time-zero). Mineral abbreviations are consistent with IMA approved mineral symbols (Warr, 2021): Sme: smectite, Mca: mica, Crs: cristobalite, Qtz: quartz, and Pl: plagioclase. Star (*) denotes isolated reflections that may correspond to carbonates or nitrate (N) likely precipitated due to the alkaline pH conditions and CO_2 atmosphere. Only main reflections are labeled.

revealed the presence of smectite and different accompanying mineral phases such as amorphous silica (separately and adsorbed on smectite), and calcite in all the treatments (Fig. 2A, B, and D, respectively). This amorphous silica could result from minor dissolution of smectite as a consequence of the interaction between the bentonite and the aqueous solution (Cappelli et al., 2018; Huertas et al., 2001). However, no U mineral phases were identified in the U treated samples, probably due to the low metal concentration assayed (1.26 mM uranyl nitrate) or the type of the method/technique used for the analyses of the U speciation in the sample (e.g. EXAFS spectroscopy).

Interestingly, HAADF-STEM and EDX analyses revealed the presence of a bright mineral structure constituting iron sulfide (Fe and S peaks) accompanied by smectite (Si, Al, Mg, and Ca peaks) in the U treated microcosms (Fig. 2D and E). This iron sulfide probably occurred in pyrite (FeS_2) as an accessory mineral in the bentonite. Pyrite would act as a sulfide source to corrode metal waste canisters (e.g. copper) and thus, compromising DGR safety. Nevertheless, it was previously reported that corrosion of Cu-canisters by pyrite might differ depending on the bentonite barrier. However, this was not tested in all of the bentonites (Kaufhold et al., 2017). Bentonites have a high microbial diversity including sulfate reducing bacteria (SRB) (Lopez-Fernandez et al., 2015; Svensson et al., 2011) that produce sulfide whose oxidation is coupled with ferric iron mineral reduction. The resultant ferrous iron could react with free sulfides to produce iron sulfide (Pedersen et al., 2017). Therefore, the iron sulfides observed in these samples could have originated from microbiological and/or geochemical processes.

3.2.2. *VP-FESEM analyses of colored spots in the bentonite microcosms*

Spots of differing color, size, and quantity were observed in all treated anaerobic microcosms (Fig. 3). The color varied depending upon the type of bentonite treatment with a darker color (black) in the non-G2P treated samples (H, N, and U) and orange brown in the G2P-treated microcosms (G, GN, and GU). The largest spots were identified in GU microcosms while poorly discernable ones were observed in U samples. The wide range of sizes was in turn observed in GN, G, N, and H samples. In general, the number of surface spots was highly different between the treatments, with more spots in the GN microcosms (Fig. 3).

VP-FESEM analyses showed typical smectite leaf-like morphologies (Fig. 4A and E). However, analyses of these colored spots highlighted some areas with a high atomic number being brighter than others (Fig. 4B and F, indicated by arrows). Composition analysis of these areas gave EDX spectra with high peaks of Mn and O, in addition to Si, Al, Mg, and Na that corresponded to smectites (Fig. 4A). EDX maps showed the elemental distribution in the bentonite particles of Mn, associated with the brighter areas (Fig. 4C, D, G, and H) that likely corresponded to Mn oxides attached to bentonite. On the one hand, sorption of Mn in bentonites has previously been reported in several works (Al-Jariri and Khalili, 2010; Dolinská et al., 2015; Iskander et al., 2011). As an example, Iskander et al. (2011) reported that the amount of Mn adsorbed ranged between 9.83% and 33.24% of the total Mn added. On the other hand, although structural properties can be affected, bentonite provides an efficient surface for the Mn oxides due to their large surface area (Dolinská et al., 2015). At pre-incubation time, bentonite microcosms were shown to be composed of 0.02 ppm MnO through X-Ray Fluorescence (XRF) as it was described in Povedano-Priego et al. (2019), and no speckles were observed on the surface. The colored spots and the precipitates observed in VP-SEM after incubation could correspond to Mn(IV) oxides, recently reported as being dark brown colored (Kitjanukit et al., 2019), resulting from a Mn(II) oxidation. Liu et al. (2018) reported that microbial reoxidation of Mn(II) to Mn(IV) may occur, although Mn(II)-oxidizing bacteria are aerobic and the limiting O_2 conditions affect their activity. Moreover, fungi isolated from acid mine drainage treatment systems have been described for their ability to oxidize Mn(II) forming MnO_2 mineral phases under aerobic conditions (Santelli et al., 2011). Several fungal strains related to *Penicillium*, *Fusarium*, *Talaromyces, Alternaria, Aspergillus,* and *Aureobasidium* were isolated from the U treated bentonite microcosms under aerobic conditions (Morales et al., 2019). Fungi could play a role in the oxidation of Mn(II), such as *Fusarium oxysporum* (Huy et al., 2017), *Phaeoacremonium* spp. (Overton et al., 2006), *Alternaria* sp., and *Acremonium* sp. (Hansel et al., 2012). In addition, VP-FESEM images revealed the presence of fungal mycelia associated with MnO_2 (Fig. 4G). However, there is still a lack of information in the literature concerning oxidation of Mn(II) to Mn(IV) under anaerobic conditions. This potential formation of Mn oxides in bentonite would need further investigation in the future since Mn oxides were reported to play a role in the immobilization of U(VI) through sorption mechanisms producing a decrease in the U solubility (Ren et al., 2020; Soo Lee et al., 2015). In fact, analyses of the spots in the U-treated microcosms by VP-SEM and EDX techniques indicated the presence of both U and Mn in several areas (Fig. 5, arrows). Ren et al. (2020) reported the uranium-sorption capacity of the Mn oxides, which reached its highest value at 280 mg g^{-1} by forming inner-sphere bidentate binuclear structure. Therefore, more research is required on this process and the origin of the colored precipitates in bentonite microcosms under anaerobic conditions.

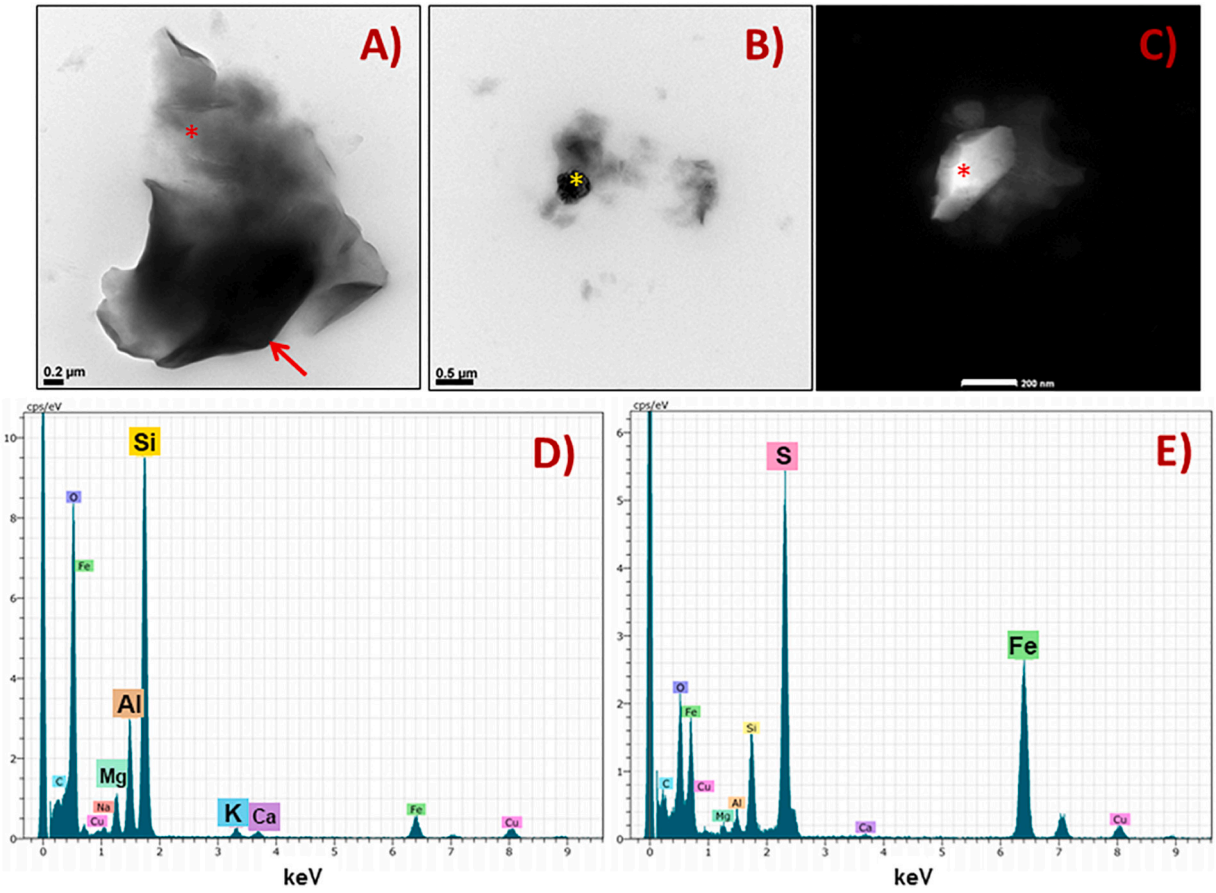

Fig. 2. High Resolution Transmission Electron Microscopy (HRTEM) micrographs (A and B) and High-Angle Annular Dark-Field Scanning Transmission Electron Microscopy (HAADF-STEM) imaging (C) of minerals in the anaerobic bentonite microcosms. Smectite (A, arrow), amorphous silica (A, asterisk), calcite (B, asterisk), and pyrite (C, asterisk) are shown. EDX spectra indicate the composition of smectite (D) and pyrite (E).

3.3. Microbial diversity and community structure in the anaerobic microcosms

Total community DNA from the microcosms was extracted and sequenced. A mean of 3715 sequences per sample was annotated obtaining 790 OTUs classified into phylum (93.9% of phylotypes), class (89.1% of phylotypes), order (87.9% of phylotypes), family (76.1% phylotypes), and genus (42.2% phylotypes) levels. According to the high values of ShannonD (higher index values correspond to higher diversity) and SimpsonD ($\geq$0.91, ranging from 0 to 1, being 1 the maximum diversity and 0 a unique OTU) indices, a high bacterial diversity was found and a nearly uniform distribution (ShannonE index $\geq$0.78) of OTUs was reached in all microcosms (Table 1).

Bacterial PCoA community structure analysis at the genus level (Fig. 6) suggested the G2P/uranyl nitrate-treated samples (GU2 and GU3) had a unique diversity compared to the other microcosms that further clustered into G2P and G2P/sodium nitrate-treated samples (G2, G3, GN1, and GN3; represented with blue circle) and samples with no G2P treatment (H1, H2, N1, N2, U2, and U3; represented with black circle). Therefore, the concomitant presence of U and G2P had a pronounced effect on the bacterial community of the bentonite microcosms. In addition, the heatmap supported the clustering of the treated microcosms shown by the PCo analysis, with the highest relative abundance of the taxa *Ralstonia*, *Pseudomonas*, *Marinobacter*, *Desulfovibrio*, *Sulfuritalea,* unclassified Desulfobulbaceae, and *Candidatus Falkowbacteria* in GU microcosms (Fig. 7).

The annotated OTUs (Fig. 8, Supplementary Figs. S3 and S4, Supplementary Table S2, Supplementary Data S1 and S2) were taxonomically related to 29 bacterial phyla with Proteobacteria as the dominant phylum (47–73% of the total community relative abundance) followed by Bacteroidetes with a mean relative abundance of 13.9% (Fig. 8, Supplementary Table S2). Fig. 8 showed the identified bacterial phyla with a relative abundance above 0.15% in at least one of the replicates; the minority phyla (a total of 9) were grouped in the category "Others", which includes Nitrospirae, Lentisphaerae, Thermotogae, and Armatimonadetes, among others (Supplementary Table S2). Whilst Actinobacteria constituted 0.6% of the bacterial community in the anaerobic microcosms, this phylum was identified as one of the most abundant taxa in the previous experiment under oxic conditions (Povedano-Priego et al., 2019). This difference could be explained since most Actinobacteria are aerobic, although some genera are adapted to anaerobic conditions, such as marine Actinobacteria (Anandan et al., 2016). In addition, the presence of strictly anaerobic bacteria mainly from genera *Desulfatiglans* and *Clostridium* (Supplementary Fig. S4, Supplementary Data S1) in the anaerobic microcosms contrasts with their total absence in previous aerobic experiments of the same set-up (Povedano-Priego et al., 2019).

The non-G2P-treated microcosms were dominated by Proteobacteria with high average relative abundances in the water- (H; 71.6%), nitrate- (N; 70.3%), and uranium- (U; 47.3%) treated microcosms (Fig. 8, Supplementary Table S2) with Gamma- (52.8, 39.2, and 21.3%) and Deltaproteobacteria (11.8, 14.2, and 23.3%) being the most abundant classes (Supplementary Fig. S3, Supplementary Data S2). Other concurrent phyla were Bacteroidetes (9.8, 6.1, and 15.2%), Cyanobacteria (7.8, 7.4, and 8.1%), Epsilonbacteraeota (2.2, 7.4, and 8.4%), and Firmicutes (0.8, 1.4, 4.6%). At the genus level, *Sulfurimonas* (1.7, 3.4, and 7.6%), unclassified Desulfobacteraceae (2.4, 2.3, and 6.8%), *Desulfatiglans* (0.1, 4.6, and 6.7%), *Clostridium* (0.8, 2.3, and 4.5%), *Candidatus*

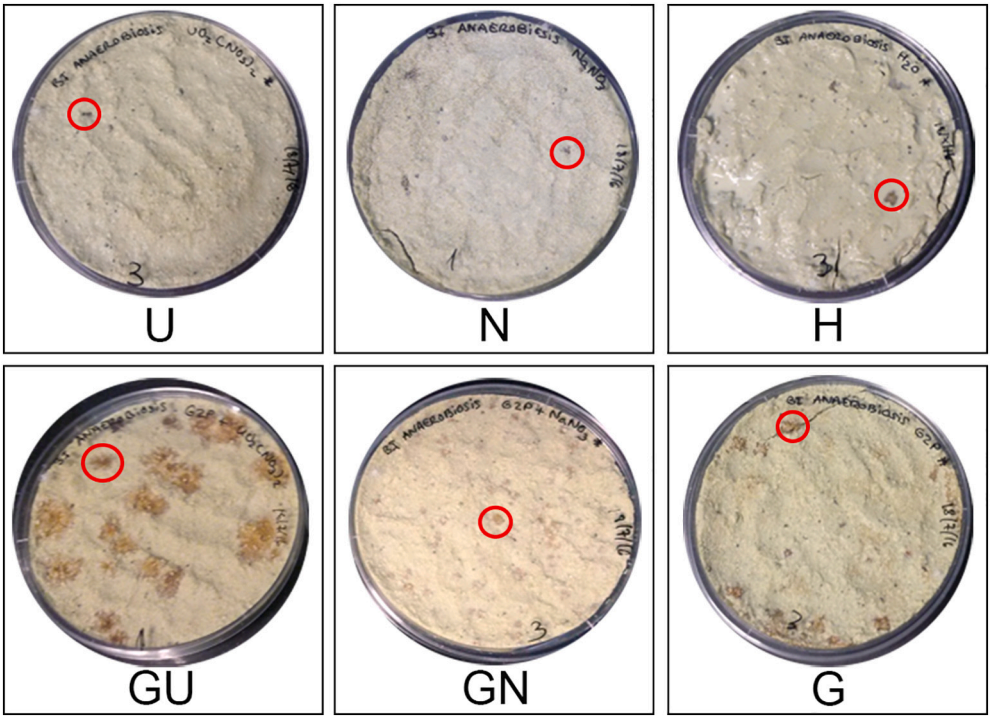

Fig. 3. Plates of bentonite microcosms showing different colored spots after six months incubation under anaerobic conditions. The microcosms were treated with uranyl nitrate (U), sodium nitrate (N), distilled water (H), G2P + uranyl nitrate (GU), G2P + sodium nitrate (GN), and G2P (G). The brown spots are indicated by red circles in the microcosms. (For interpretation of the references to color in this figure legend, the reader is referred to the web version of this article.)

Electrothrix (1.6, 2.3, and 4.2%), and unclassified Flavobacteraceae (1.2, 3.4, and 2.7%) were most abundant in H, N, and U samples, respectively (Supplementary Fig. S4, Supplementary Data S1). Being strict or facultative anaerobic bacteria, these microorganisms have been recognized previously for their successful growth under anaerobic conditions (Bernardet and Nakagawa, 2006; Hung et al., 2011; Kuever, 2014; Takai et al., 2006; Xie and Müller, 2018).

As for the G2P-treated microcosms, Proteobacteria dominated the G2P (G), G2P/sodium nitrate (GN), and G2P/uranyl nitrate (GU) treatment communities with 46.7, 55.2, and 72.9%, respectively (Fig. 8, Supplementary Table S2). In contrast to the non-G2P-treated microcosms, the second most abundant phylum was Patescibacteria accounting for 13.9, 8.0, and 10.5% of G, GN, and GU bacterial communities, respectively, followed by Bacteroidetes (13.9, 3.1, and 2.8%), Spirochaetes (1.7, 8.5, and 1%), and Cyanobacteria (3.2, 1.1, and 2.2%). The corresponding classes of these phyla were ABY1 from the Patescibacteria (13.9, 8.0, and 10.2%), Bacteroidia (6.2, 2.6, and 2.7%), Spirochaetia (1.7, 7.4, and 0.8%), and Oxyphotobacteria (3.2, 1.1, and 2.2%) representing >2% of the total community (Supplementary Fig. S3, Supplementary Data S2).

According to the relative abundances of genera, the most different bacterial community was shown in GU microcosms with respect to the other treatments (Supplementary Fig. S4, Supplementary Data S1). *Ralstonia* (18.2%), *Pseudomonas* (9.2%), *Marinobacter* (8.8%), *Desulfovibrio* (7.4%), *Immundisolibacter* (6.9%), and *Sulfuritalea* (4.6%) were the most abundant genera in GU microcosms but little or no presence of these genera was detected in the G and GN controls (Supplementary Fig. S4, Supplementary Data S1). In addition, families belonging to unclassified Deltaproteobacteria (Marine group B; 1.51 and 19.8%), Desulfobulbaceae (18.1 and 5.3%), Spirochaetaceae (0.9 and 10.3%), *Candidatus Falkowbacteria* (20.9 and 1.4%) and Methylophilaceae (4.5 and 5%) were detected with higher relative abundance in G and GN microcosms than in the others.

3.4. Potential impact of bacterial community of anaerobic microcosms on the nuclear waste storage

One-Way ANOVA ($n = 2$ per treatment, $p < 0.05$) statistical analyses were performed for the OTUs with >1% relative abundance to determine the potential influence of uranium, G2P, and nitrate treatments on the indigenous bacterial community of bentonite. At the phylum level, significant differences were found for e.g. Cyanobacteria, Firmicutes, and Spirochaetes (Supplementary Data S3). Regarding the classes with >0.1% relative abundance, Deltaproteobacteria, Oxyphotobacteria, Clostridia, Fusobacteriia, Leptospirae, and Oligosphaeria were significantly different (Supplementary Data S4). Analyzing the genera with 1% in at least one sample, significant differences were obtained for 28 genera (including unclassified bacteria) such as *Ralstonia*, *Pseudomonas*, *Desulfovibrio*, *Marinobacter*, *Sulfurimonas*, *Desulfatiglans*, unclassified genus belonging to Marine Group B (Deltaproteobacteria), *Candidatus Falkowbacteria,* and Desulfobulbaceae, among others (Supplementary Data S5).

3.4.1. Impact of nitrate treatment on the bacterial community of the anaerobic microcosms

Nitrate can be reduced to N_2 through anaerobic denitrification after oxygen has been fully consumed in the DGR (Kutvonen et al., 2015). The introduction of nitrogen compounds such as nitrate during DGR construction (e.g. by blasting activity and other mechanical processes) may enhance the growth of several groups of microorganisms (Kutvonen et al., 2015; Rajala et al., 2015). Therefore, in this study the effects of nitrate on the structure and composition of the bentonite bacterial community under anoxic atmosphere have been determined, both for N and GN microcosms in comparison with their respective controls (H and G microcosms, respectively). Only the phylum Spirochaetes and Spirochaetaceae family had significantly increased their relative abundance in GN samples in comparison with the other samples (Tukey post-hoc test, $n = 2$ per treatment, $p < 0.045$; Fig. 8, Supplementary Fig. S4, Supplementary Data S6-S8). This family encompasses members able to

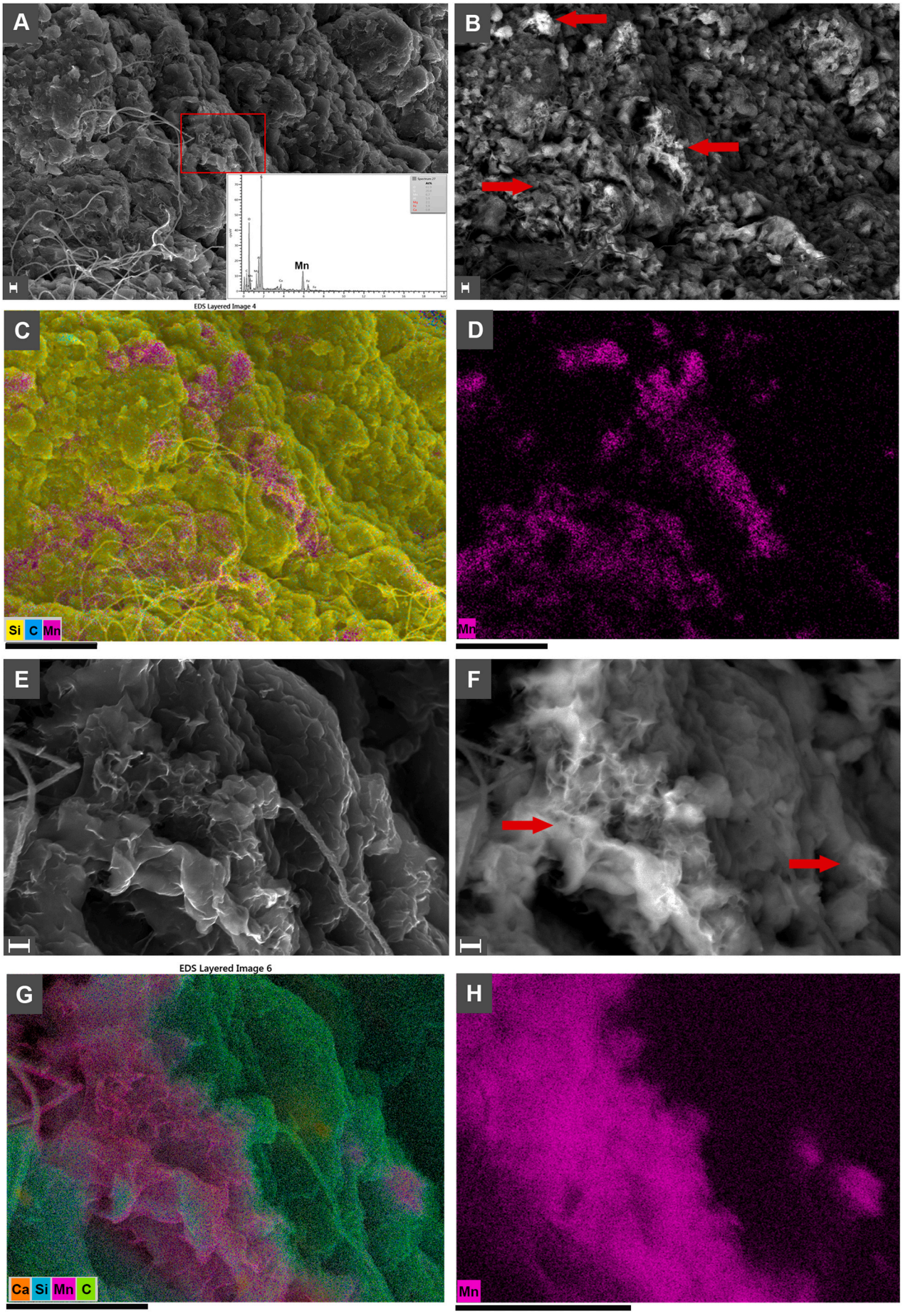

(caption on next page)

Fig. 4. VP-FESEM and EDX map images of brown spots in anaerobic G2P-sodium nitrate treated microcosms (GN). Images shown in secondary electrons with the InLens detector of the bentonite samples (A and E) and images shown in backscattered electrons with the AsB detector (B and F). The red square area in A was amplified in E and F. Bright areas with high atomic number are indicated by arrows in B and F. EDX layered maps corresponding to images A and B with represented Si, C, and Mn signals (C) and only with Mn signal (D). EDX layered maps corresponding to images E and F with represented Ca, Si, C, and Mn signals (G) and only with Mn signal (H). Scale bar represents 2 μm in A and B, 25 μm in C and D, 1 μm in E and F, and 10 μm in G and H. (For interpretation of the references to color in this figure legend, the reader is referred to the web version of this article.)

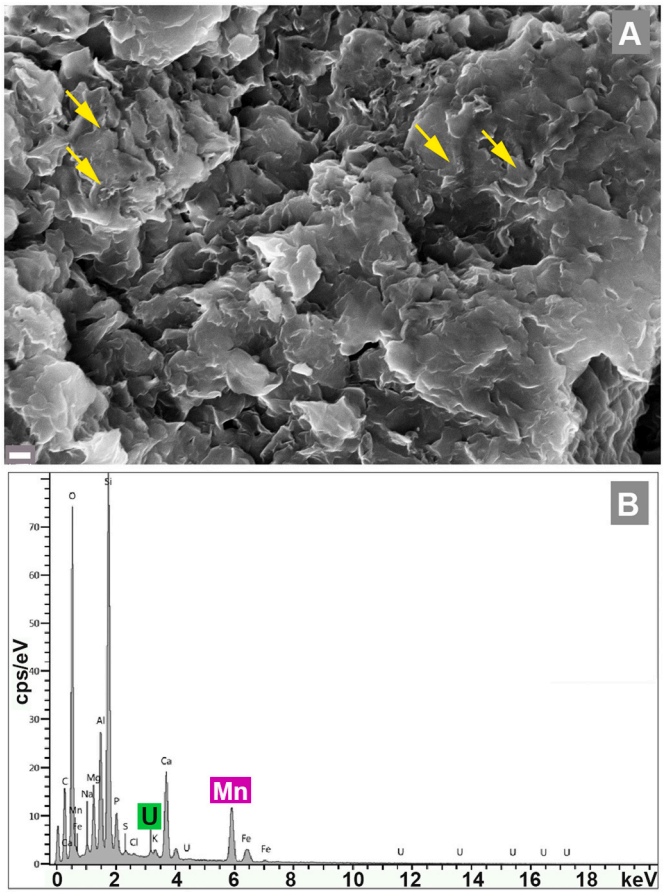

Fig. 5. VP-FESEM and EDX analyses of colored spots in anaerobic uranium-treated microcosms (U). A) Image shown in secondary electrons with the InLens detector of the bentonite samples. B) EDX spectrum performed in the bentonite sample indicated by arrows in A. Scale bar represents 1 μm.

Table 1
Alpha-diversity indices of anaerobic bentonite microcosms.

Sample	S	ShannonD	ShannonE	SimpsonD	Good's coverage
H	71.1	549.5	0.89	0.97	0.78
N	81	575.9	0.91	0.98	0.70
U	84.2	575.6	0.90	0.98	0.67
G	39	413.9	0.78	0.91	0.89
GN	45	428.3	0.78	0.91	0.86
GU	31	41.8	0.84	0.93	0.94

Richness index (S), diversity indices (ShannonD and SimpsonD), evenness index (ShannonE), and Good's coverage values are shown.

anaerobically reduce nitrate to nitrite such as *Spirochaeta aurantia* and *S. halophila* (Leschine and Paster, 2015). Furthermore, Saad et al. (2017) reported a strong effect of a nitrate treatment on the microbial community of marine sediments, favoring the development of fermentative bacteria including *Spirochaeta* species. Several microorganisms described for their nitrate reduction capacity were detected in the anaerobic microcosms. Comparing GN and G samples, both the unclassified Deltaproteobacteria Marine Group B ($p < 0.002$) and *Limnobacter* ($p < 0.022$) had significantly higher relative abundances in GN microcosms (Supplementary Data S8). *Limnobacter* utilizes nitrate or nitrite as a nitrogen source through nitrate/nitrite reduction (Chen et al., 2016). *Flavobacterium* and other unclassified members belonging to Flavobacteriaceae were more abundant in microcosms containing nitrate. This family includes species capable of nitrate reduction such as *Flavobacterium denitrificans* (Broman et al., 2017; Sun et al., 2009). The nitrate-reducing bacteria could positively affect uranium reduction in the DGR by first consuming the available nitrate before species capable of uranium reduction are selected (Safonov et al., 2018). However, the presence of some denitrifying bacteria could contribute to the oxidation of previously immobilized U(IV) into soluble U(VI) using nitrate as terminal electron acceptor (Wu et al., 2010).

To further visualize statistically significant taxa in all anaerobic microcosms, LEfSe (LDA Effect Size) analysis was performed (Fig. 9). Significant taxa related to nitrate treatment are shown in green (for GN) or light blue (for N). Some of the nitrate reducers were found significant ($p < 0.05$) in these samples such as Spirochaetacea family (GN), *Limnobacter* (GN), and *Brevundimonas* (N).

3.4.2. Impact of glycerol-2-phosphate on the bacterial community in the anaerobic bentonite microcosms

The G2P amendment could introduce changes to the composition of the bacterial community, enhancing the relative abundance of bacteria able to use glycerol as carbon source (Fig. 8 and Supplementary Fig. S4). At the phylum level, only Spirochaetes were enriched significantly in GN microcosms (Tukey post-hoc test, $n = 2$ per treatment, $p = 0.027$) in comparison to the N microcosms along with Deltaproteobacteria at the class level ($p = 0.026$; Supplementary Data S6 and S7). However, in the previous experiment under aerobic conditions more significant differences were observed between G2P-treated and non-G2P-treated microcosms (Povedano-Priego et al., 2019). This greater effect of G2P under oxic conditions could be due to the fact that dissimilatory aerobic oxidation of glycerol is more favorable compared to assimilation under reducing conditions (Kang et al., 2014). Nevertheless, some bacteria are able to utilize glycerol anaerobically as a carbon source for their growth such as *Escherichia coli* and members of Clostridia (e.g., *Clostridium* spp. and *Anaerobium acetethylicum*) to produce ethanol, hydrogen, formate, butyrate, and acetate (Biebl, 2001; Patil et al., 2016). At the genus level, 15 out of 100 statistically analyzed genera with >1% of relative abundance in at least one sample were significantly ($p < 0.05$) more abundant in G2P-treated samples than in the controls. These included *Pseudomonas*, *Desulfovibrio*, *Marinobacter*, *Limnobacter*, *Desulfatiferula*, *Hoeflea*, *Candidatus Falkowbacteria*, and some unclassified genera belonging to Desulfobulbaceae, Lentimicrobiaceae, and Deltaproteobacteria Marine Group B (Supplementary Data S8). The presence of *Desulfovibrio* spp. in these microcosms was notable since several species of this genus utilize glycerol as an electron donor (Ben Ali Gam et al., 2018; Qatibi et al., 1998), generating acetate and reducing sulfate as the terminal electron acceptor (Qatibi et al., 1998). The resulting acetate could be used as an energy source by other groups of bacteria such as the iron-reducing bacteria from the family Geobacteraceae. In fact, members of this family have been detected often with high abundance in subsurface environments after stimulation of concomitant U(VI) and Fe(III) reduction by the addition of acetate as electron donor (Petrie et al., 2003).

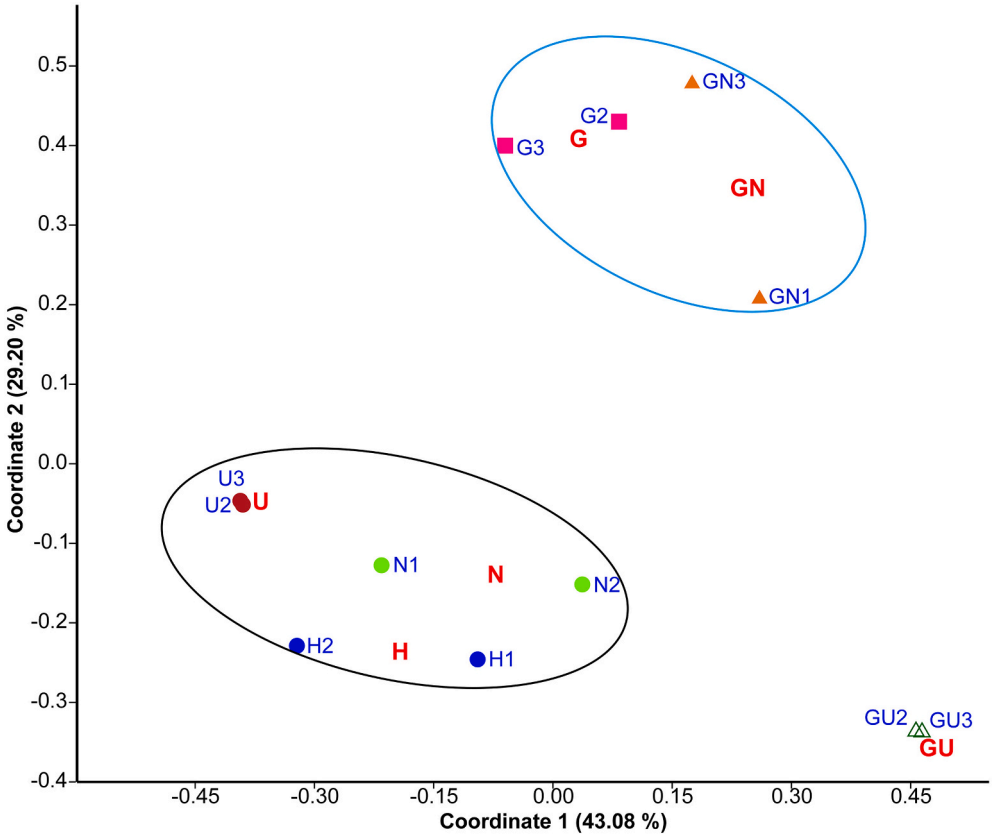

Fig. 6. Principal Coordinate Analysis (PCoA) plot comparing the bacterial community structure at genus level of the different treated microcosms (showing duplicates). Abbreviations: (H) Distilled water, (N) sodium nitrate, (U) uranyl nitrate, (G) glycerol-2-phosphate (G2P), (GN) G2P and sodium nitrate, and (GU) G2P and uranyl nitrate treated samples. Represented are two clusters: G2, G3, GN1, and GN3 (blue circle); and H1, H2, N1, N2, U2, and U3 (black circle). The percentage variation explained by Coordinates 1 and 2 are indicated on the axes. (For interpretation of the references to color in this figure legend, the reader is referred to the web version of this article.)

3.4.3. Impact of uranium on the bacterial diversity in the anaerobic bentonite microcosms

Analyzing the bacterial community in the uranium-amended microcosms, an increase in the relative abundance of the phylum Firmicutes (4.6%) was observed in the U microcosms compared to the 1.4% in the N samples (Fig. 8, Supplementary Table S2). Members of Firmicutes have been previously detected in U-containing samples (Khan et al., 2013; Lopez-Fernandez et al., 2018; Povedano-Priego et al., 2019) with 24% of the total bacterial community in a uranium mine tailings-water interface (Khan et al., 2013). In addition, Firmicutes was found to be dominant in U samples under aerobic conditions (Lopez-Fernandez et al., 2018). Lentisphaera, Thermotogae, and Candidate bacterial phylum BRC1 were identified at a significant level in U samples but with minor relative abundance compared to the N microcosms (Supplementary Table S2, and Supplementary Data S6). Lentisphaera belong to the Planctomycetes-Verrucomicrobia-Chlamydia super-phylum, which has been identified in heavy metal polluted soils (Hemmat-Jou et al., 2018; Yilmaz et al., 2016; Youssef and Elshahed, 2014).

The relative abundances of the classes Leptospirae (belonging to Spirochaetes) and Clostridia (affiliated with the Firmicutes) were significantly higher in U samples comparison to N controls ($p < 0.05$; Fig. S3, Supplementary Data S7). The Clostridia class is prevalent in sediments, soils, and even radioactive wastes and plays a key role in reducing soluble U(VI) to insoluble U(IV) species (Francis and Dodge, 2008; Newsome et al., 2014a). Furthermore, the genus *Clostridium* was more abundant in U microcosms than in N samples with 4.5% of relative abundance (Supplementary Data S1). Gao and Francis (2008) reported the ability to reduce U(VI) to U(IV) in a nitrate independent process of several species of *Clostridium* previously exposed to uranyl nitrate under anaerobic conditions. However, this is in contrast to other studies that show nitrate can act as an oxidizer of U(IV) through different mechanisms: 1) abiotic oxidation by intermediates in denitrification such as nitrite, 2) direct oxidation coupled to nitrate reduction by bacteria, or 3) oxidation by Fe(III) produced through denitrification (Newsome et al., 2014a). Moreover, in the presence of H_2 not only vegetative cells but also spores of *Clostridium* are able to reduce U(VI) enzymatically, producing a U(IV) precipitate located in the exosporium as well as between spores (Vecchia et al., 2010). *Sulfurimonas*, *Desulfatiglans*, *Hyphomonas*, and unclassified Lentimicrobiaceae were significantly more abundant ($p < 0.045$) in U microcosms in comparison to N controls (Supplementary Data S8). The LefSe plot also highlighted (orange color) the significant abundance of *Clostridium*, *Sulfurimonas*, and *Desulfatiglans* in U microcosms (Fig. 9).

Sulfurimonas contributes to the formation of sulfate by oxidation of sulfide coupled to the complete reduction of nitrate to N_2, according to the following equation (Handley et al., 2013); in this case, nitrate comes from uranyl nitrate:

$$8NO_3^- + 5S^{2-} + 8H^+ \rightarrow 4\,N_2 + 5SO_4^{2-} + 4H_2O$$

The generated sulfate may be used by sulfate-reducing bacteria (SRB) such as *Desulfatiglans* (Jochum et al., 2018). Grigoryan et al. (2018) also reported the presence of SRB in different bentonites, predominating *Desulfosporosinus* in the MX-80 bentonite. *Sulfurimonas* also possesses proteins that could play a role in heavy metal tolerance (Han and Perner, 2015).

Among the 100 analyzed genera of the bacterial community in GU microcosms, *Ralstonia* (18.2%), *Pseudomonas* (9.2%), *Marinobacter* (8.8%), *Desulfovibrio* (7.4%), *Immundisolibacter* (6.9%), *Sulfuritalea* (4.6%), *Hyphomonas* (1.4%), and *Pseudoalteromonas* (1.2%) were significantly more abundant in GU microcosms than in GN controls (Tukey post-hoc test, $n = 2$ per treatment, $p < 0.05$; Supplementary Data S1 and S8). In comparison with the rest of samples, the GU treatment had more significant taxa in terms of relative abundance including the above mentioned *Desulfovibrio*, *Pseudomonas*, *Ralstonia*, and *Marinobacter* (Fig. 9). *Ralstonia* is reported to be enhanced in nitrate-treated microcosms due to its capacity to use nitrate as terminal electron

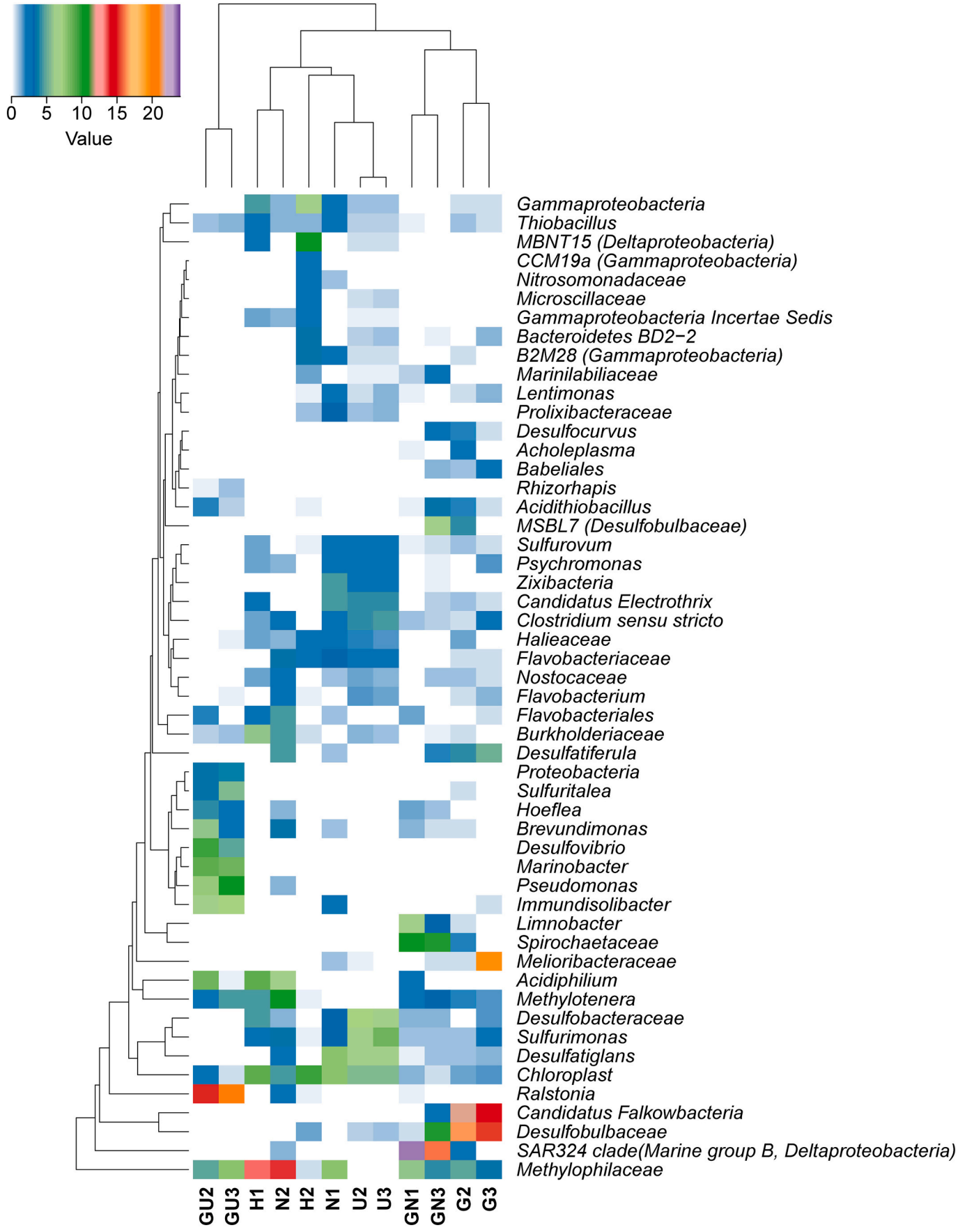

Fig. 7. Heatmap of the relative abundance from 16S rRNA sequencing outputs with clustering based on Manhattan distance and average linkage for both columns and rows throughout the sample set. The relative abundance of the taxa was as indicated in the color bar.

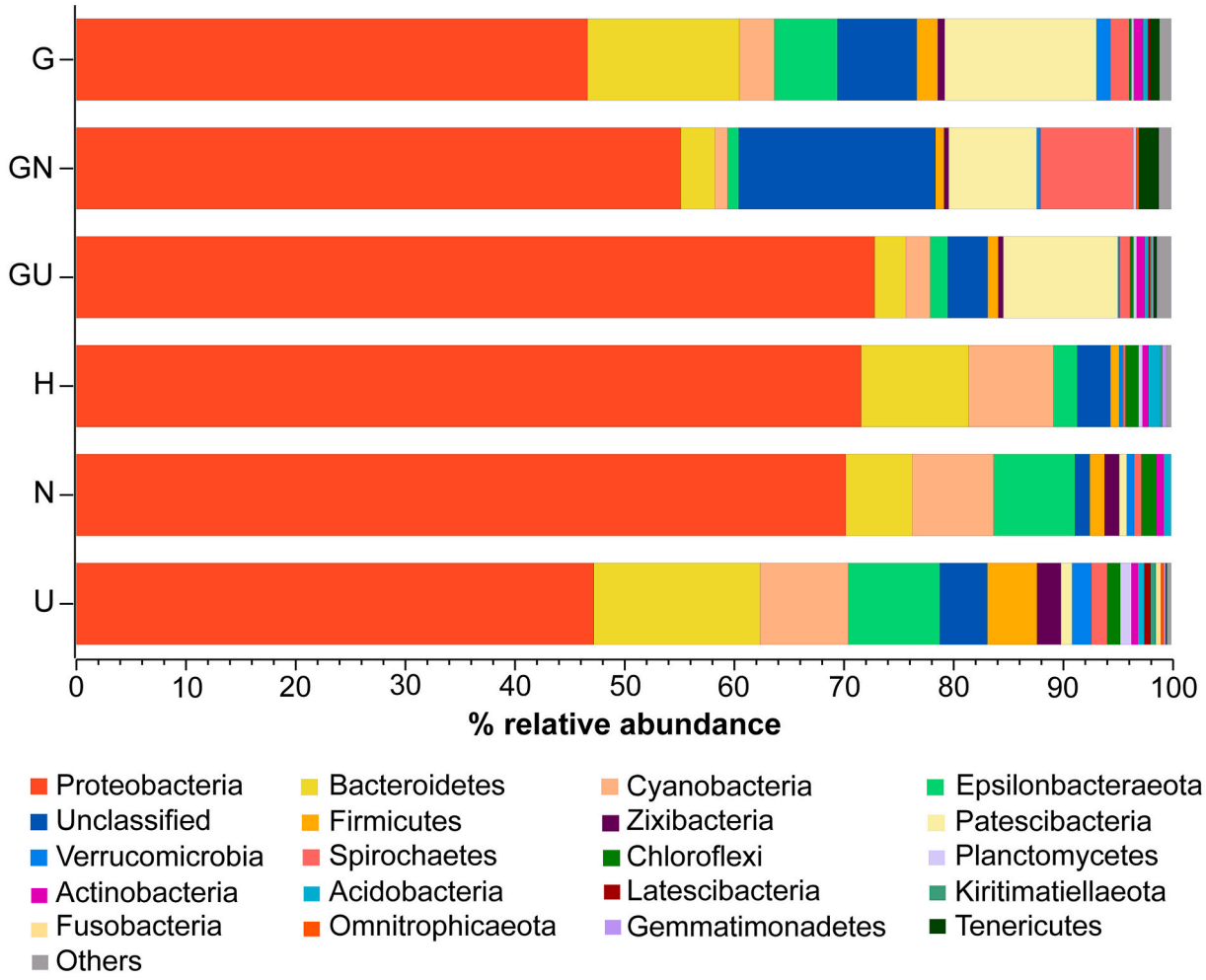

Fig. 8. Average relative abundance of phyla from duplicate treated bentonite microcosms. Abbreviations: (H) Distilled water, (N) sodium nitrate, (U) uranyl nitrate, (G) glycerol-2-phosphate (G2P), (GN) G2P and sodium nitrate, and (GU) G2P and uranyl nitrate treated samples. Colors were assigned to each phylum according to their relative abundance (the most abundant first by line). The category "others" (grey color) includes the rest of identified phyla with <0.15% of relative abundance.

acceptor (Lopez-Fernandez et al., 2018). In addition, *Ralstonia* has been isolated from uranium contaminated sites (Brzoska and Bollmann, 2016; Salome et al., 2013). The denitrifying *Pseudomonas* species are well-known for their capacity to interact with uranium through different mechanisms such as biosorption, intracellular accumulation, biomineralization, and bioreduction that contribute to U immobilization (Chabalala and Chirwa, 2010; D'Souza et al., 2006; Hu et al., 1996; Kazy et al., 2009; Kazy et al., 2008; Newsome et al., 2014b). Biosorption of uranium by *P. aeruginosa* and *P. fluorescens* is demonstrated in several studies by detection of uranium in the entire outer membrane-peptidoglycan-plasma membrane complex (Hu et al., 1996; Merroun et al., 2005). In addition to biosorption using the whole cell, extracellular polysaccharide excreted by *P. aeruginosa* is able to bind U through carboxylic groups (Kazy et al., 2008). Further uranium-*Pseudomonas* interaction mechanisms are bioaccumulation (accumulation of the metal in the cytoplasm by microorganisms) via increased membrane permeability allowing metal diffusion into the cells (Kazy et al., 2009; König et al., 2010) and sequestration of uranium through a biomineralization process in which the uranium is precipitated as crystalline U-phosphates (Choudhary and Sar, 2011; Kazy et al., 2009). In turn, under anaerobic and reducing conditions, *Pseudomonas* spp. have the capacity to reduce soluble U(VI) to the more insoluble U(IV) form (Chabalala and Chirwa, 2010; Newsome et al., 2015; Newsome et al., 2014b). In addition to *Pseudomonas*, *Desulfovibrio* also has been studied extensively for its capacity to reduce hexavalent uranium (Heidelberg et al., 2004; Lovley et al., 1993; Payne et al., 2002; Stylo et al., 2015). The mechanism to reduce U(VI) by *Desulfovibrio* is potentially a redox reaction, which involves the oxidation of an electron donor (e.g. acetate, lactate) to CO_2, coupled to the reduction of U(VI) to U(IV), producing the precipitation of uraninite. This is an enzymatically mediated process where U(VI) reductases such as the periplasmatic *c*-type cytochrome are involved (Heidelberg et al., 2004; Newsome et al., 2014a). Like SRB, *Pseudomonas* and *Desulfovibrio* also have the ability to indirectly reduce U(VI) by sulfide produced through sulfate reduction (Beyenal et al., 2004; Hua et al., 2006). Hua et al. (2006) reported crystalline uraninite as a result of the U(VI) reduction by hydrogen sulfide. Whilst *Pseudomonas* and *Desulfovibrio* were the most relevant genera in relation to their capacity for U immobilization found under anoxic conditions in the bacterial community of the GU microcosms, the most important genus in oxic microcosms was *Amycolatopsis*, since these Actinobacteria have the ability to immobilize U(VI) mediated by phosphatase activity through a biomineralization process producing U-phosphates (Povedano-Priego et al., 2019). Therefore, these anaerobic genera may play an important role in a DGR because of their ability to interact with and immobilize uranium, in case uranium leaks into the bentonite barrier where anaerobic conditions will prevail indefinitely, starting sometime after DGR closure.

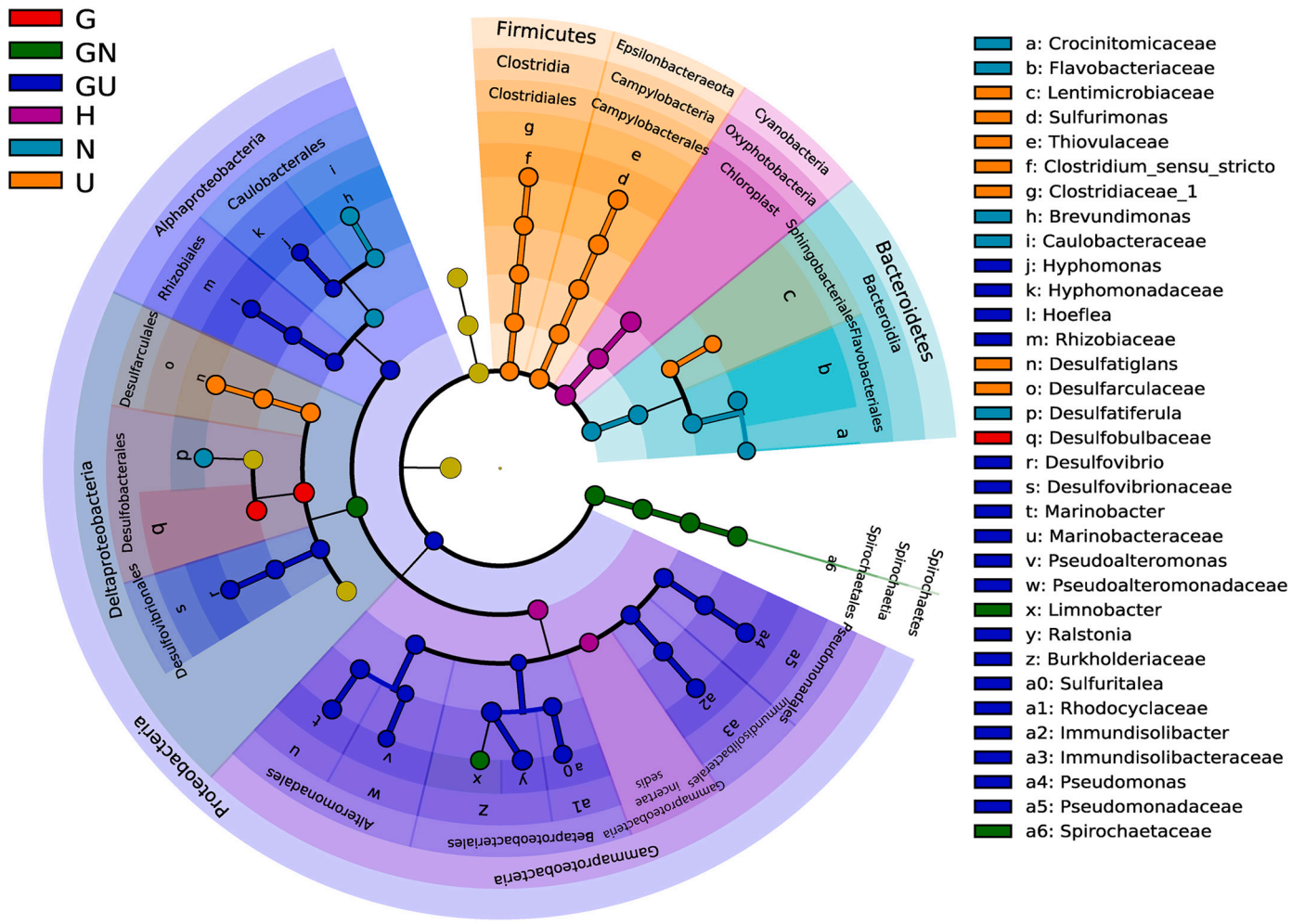

Fig. 9. Cladogram of LEfSe (LDA Effect Size) analysis showing differentially abundant taxonomic levels in each treatment with a linear discriminant analysis (LDA) score ≥ 2.0, $p < 0.05$. The data were obtained from the V3–V4 region of the 16S rRNA gene amplifications. Abbreviations: (H) Distilled water, (N) sodium nitrate, (U) uranyl nitrate, (G) glycerol-2-phosphate (G2P), (GN) G2P and sodium nitrate, and (GU) G2P and uranyl nitrate treatments. Significant taxa of G, GN, GU, H, N, and U microcosms are represented in red, dark green, blue, purple, light green, and orange, respectively. Family and genus taxonomic levels are shown in the legend. (For interpretation of the references to color in this figure legend, the reader is referred to the web version of this article.)

4. Conclusions

Despite that bentonites represent a highly oligotrophic environment (extremely nutritionally deficient conditions), a wide bacterial diversity was found in anaerobic microcosms in this study that could lead to a broad range of metabolic processes (e.g. nitrate reduction, glycerol utilization, sulfate and uranium reduction) supporting the mutual energetic and nutritional requirements within the community (e.g. glycerol may be transformed to other carbon compounds such as acetate, which could be utilized mainly for the growth of some IRB and SRB). Several indigenous bacteria were identified, in the present study, belonging to the SRB such as *Desulfovibrio*, *Desulfatiglans*, and *Desulfobulbaceae*, all of which may contribute to the formation of pyrite in the bentonite microcosms. Although no significant changes in the mineralogy of the bentonite were observed by the XRD analyses in terms of principal minerals, colored spots were observed in the microcosms probably consisting of Mn(IV) precipitates that may be produced by microbial activity. These Mn oxides could play a major role in the immobilization of U(VI) by the sequestration of this radionuclide.

One concern in the DGR is the introduction of nitrate since the presence of nitrate reducing bacteria could lead to both positive and negative circumstances: on one hand, consuming the nitrate giving way to the uranium as electron acceptor by other microorganisms; on the other hand, the nitrate reduction could result in the reoxidation of the reduced U(IV) into the more soluble U(VI). Some denitrifiers have been found significantly present in the bacterial community such as Spirochaetacea family and *Limnobacter*.

The identification of bacteria involved in the biogeochemical cycling of uranium is an important step into the safety of the DGR concept. Significant abundances of *Clostridium*, *Sulfurimonas*, and *Desulfatiglans* were found in U microcosms and *Desulfovibrio plus Pseudomonas* in GU microcosms. These bacteria may interact with this radionuclide through mechanisms such as biosorption, intracellular accumulation, biomineralization and bioreduction, depleting the toxic U(VI) from the environment. In addition, *Desulfovibrio* and *Clostridium* can utilize glycerol as a carbon source enhancing their growth and providing the necessary energy for the uranium tolerance mechanisms (e.g. bioreduction).

This study represents a part of a long-term, complex, and multidisciplinary project dedicated to highlight the microbiology of bentonites within the concept of Deep Geological Repository. Currently, several studies on the microbial community present in highly compacted bentonite have been carried out, because bentonite in a DGR would be emplaced in the form of highly compacted blocks in which presumably the microbial activity would be minimized. The present study focused on studying the interaction of uranium and bentonite microbial populations under anoxic conditions simulating a worst-case scenario in which

compaction would be altered at some location in a DGR (e.g. possibly at interfaces between bentonite blocks and the rock or canisters, between bentonite blocks, or by some unforeseen loss of bentonite), while at the same time a leak is occurring in the DGR that releases uranium and other radionuclides to the environment.

Fundings sources

This work was funded by the ERDF-financed Grant CGL2014-59616-R (80% funding by FEDER), (Ministerio de Ciencia e Innovación, España) as well as by an FPU 14/04263 ("Formación de Profesorado Universitario") grant to the first author from the Spanish Ministry (Ministerio de Educación Cultura y Deporte, MECD).

Declaration of Competing Interest

The authors declare that they have no known competing financial interests or personal relationships that could have appeared to influence the work reported in this paper.

Acknowledgements

We acknowledge the assistance of María del Mar Abad Ortega (STEM technician), Isabel Guerra Tschuschke (VP-FESEM technician), Concepción Hernández-Castillo (preparation of samples for microscopic analyses), and members of Centro de Instrumentación Científica (University of Granada, Spain). XRD analyses were performed at Instituto Andaluz de Ciencias de la Tierra, CSIC-University of Granada, Spain, with assistance of Eduardo Flores. High-throughput sequencing was carried out at the National Genomics Infrastructure hosted by the Science for Life Laboratory (Sweden). Bioinformatics analyses were carried out utilizing the Uppsala Multidisciplinary Center for Advanced Computational Science (UPPMAX) at Uppsala University (projects b2013127 and SNIC 2019/3-22). The computations were enabled by resources provided by the Swedish National Infrastructure for Computing (SNIC) at UPPMAX partially funded by the Swedish Research Council through grant agreement no. 2016-07213. MD thanks The Swedish Research Council (contract 2018-04311) for support.

Appendix A. Supplementary data

Supplementary data to this article can be found online at https://doi.org/10.1016/j.clay.2021.106331.

References

Alessi, D.S., Uster, B., Veeramani, H., Suvorova, E.I., Lezama-Pacheco, J.S., Stubbs, J.E., Bargar, J.R., Bernier-Latmani, R., 2012. Quantitative separation of monomeric U(IV) from UO_2 in products of U(VI) reduction. Environ. Sci. Technol. 46, 6150–6157. https://doi.org/10.1021/es204123z.

Al-Jariri, J.S., Khalili, F., 2010. Adsorption of Zn(II), Pb(II), Cr(III) and Mn(II) from water by Jordanian bentonite. Desalination Water Treat. 21, 308–322. https://doi.org/10.5004/dwt.2010.1623.

Anandan, R., Dharumadurai, D., Manogaran, G.P., 2016. An introduction to Actinobacteria. In: Actinobacteria - Basics and Biotechnological Applications. https://doi.org/10.5772/62329.

Anderson, C., Johnsson, A., Moll, H., Pedersen, K., 2011. Radionuclide geomicrobiology of the deep biosphere. Geomicrobiol J. 28, 540–561. https://doi.org/10.1080/01490451.2010.507644.

Ben Ali Gam, Z., Thioye, A., Cayol, J.-L., Joseph, M., Fauque, G., Labat, M., 2018. Characterization of *Desulfovibrio salinus* sp. nov., a slightly halophilic sulfate-reducing bacterium isolated from a saline lake in Tunisia. Int. J. Syst. Evol. Microbiol. 68, 715–720. https://doi.org/10.1099/ijsem.0.002567.

Bengtsson, A., Pedersen, K., 2017. Microbial sulphide-producing activity in water saturated Wyoming MX-80, Asha and Calcigel bentonites at wet densities from 1500 to 2000 $kg{\cdot}m^{-3}$. Appl. Clay Sci. 137, 203–212. https://doi.org/10.1016/j.clay.2016.12.024.

Bernardet, J.-F., Nakagawa, Y., 2006. An introduction to the family Flavobacteriaceae. In: Dworkin, M., Falkow, S., Rosenberg, E., Schleifer, K.-H., Stackebrandt, E. (Eds.), The Prokaryotes, Proteobacteria: Delta, Epsilon Subclass, vol. 7. Springer New York, New York, NY, pp. 455–480. https://doi.org/10.1007/0-387-30747-8_16.

Bernier-Latmani, R., Veeramani, H., Vecchia, E.D., Junier, P., Lezama-Pacheco, J.S., Suvorova, E.I., Sharp, J.O., Wigginton, N.S., Bargar, J.R., 2010. Non-uraninite products of microbial U(VI) reduction. Environ. Sci. Technol. 44, 9456–9462. https://doi.org/10.1021/es101675a.

Beyenal, H., Sani, R.K., Peyton, B.M., Dohnalkova, A.C., Amonette, J.E., Lewandowski, Z., 2004. Uranium immobilization by sulfate-reducing biofilms. Environ. Sci. Technol. 38, 2067–2074. https://doi.org/10.1021/es0348703.

Biebl, H., 2001. Fermentation of glycerol by *Clostridium pasteurianum* – batch and continuous culture studies. J. Ind. Microbiol. Biotechnol. 27, 18–26. https://doi.org/10.1038/sj/jim/7000155.

Broman, E., Jawad, A., Wu, X., Christel, S., Ni, G., Lopez-Fernandez, M., Sundkvist, J.-E., Dopson, M., 2017. Low temperature, autotrophic microbial denitrification using thiosulfate or thiocyanate as electron donor. Biodegradation 28, 287–301. https://doi.org/10.1007/s10532-017-9796-7.

Brzoska, R.M., Bollmann, A., 2016. The long-term effect of uranium and pH on the community composition of an artificial consortium. FEMS Microbiol. Ecol. 92 https://doi.org/10.1093/femsec/fiv158.

Cappelli, C., Yokoyama, S., Cama, J., Huertas, F.J., 2018. Montmorillonite dissolution kinetics: Experimental and reactive transport modeling interpretation. Geochim. Cosmochim. Acta 227, 96–122. https://doi.org/10.1016/j.gca.2018.01.039.

Chabalala, S., Chirwa, E.M.N., 2010. Uranium(VI) reduction and removal by high performing purified anaerobic cultures from mine soil. Chemosphere 78, 52–55. https://doi.org/10.1016/j.chemosphere.2009.10.026.

Chen, Y., Feng, X., He, Y., Wang, F., 2016. Genome analysis of a *Limnobacter* sp. identified in an anaerobic methane-consuming cell consortium. Front. Mar. Sci. 3. https://doi.org/10.3389/fmars.2016.00257.

Choudhary, S., Sar, P., 2011. Uranium biomineralization by a metal resistant *Pseudomonas aeruginosa* strain isolated from contaminated mine waste. J. Hazard. Mater. 186, 336–343. https://doi.org/10.1016/j.jhazmat.2010.11.004.

Cologgi, D.L., Lampa-Pastirk, S., Speers, A.M., Kelly, S.D., Reguera, G., 2011. Extracellular reduction of uranium via *Geobacter* conductive pili as a protective cellular mechanism. Proc. Natl. Acad. Sci. U. S. A. 108, 15248–15252. https://doi.org/10.1073/pnas.1108616108.

Díaz-Fernández, A.M., 2004. Caracterización y Modelización Del Agua Intersticial de Materiales Arcillosos: Estudio de la Bentonita de Cortijo de Archidona. PhD Thesis. Universidad Autónoma de Madrid Editorial CIEMAT, p. 505.

Dolinská, S., Schütz, T., Znamenáčková, I., Lovas, M., Vaculíková, L., 2015. Bentonite modification with manganese oxides and its characterization. Inzynieria Miner. 2015, 213–218.

Dong, H., 2012. Clay–microbe interactions and implications for environmental mitigation. Elements 8, 113–118. https://doi.org/10.2113/gselements.8.2.113.

D'Souza, S.F., Sar, P., Kazy, S.K., Kubal, B.S., 2006. Uranium sorption by *Pseudomonas* biomass immobilized in radiation polymerized polyacrylamide bio-beads. J. Environ. Sci. Health A 41, 487–500. https://doi.org/10.1080/10934520500428377.

Edgar, R.C., 2010. Search and clustering orders of magnitude faster than BLAST. Bioinformatics 26, 2460–2461. https://doi.org/10.1093/bioinformatics/btq461.

Francis, A.J., Dodge, C.J., 2008. Bioreduction of uranium(VI) complexed with citric acid by Clostridia affects its structure and solubility. Environ. Sci. Technol. 42, 8277–8282. https://doi.org/10.1021/es801045m.

Gao, W., Francis, A.J., 2008. Reduction of uranium(VI) to uranium(IV) by Clostridia. Appl. Environ. Microbiol. 74, 4580–4584. https://doi.org/10.1128/AEM.00239-08.

Grigoryan, A.A., Jalique, D.R., Medihala, P., Stroes-Gascoyne, S., Wolfaardt, G.M., McKelvie, J., Korber, D.R., 2018. Bacterial diversity and production of sulfide in microcosms containing uncompacted bentonites. Heliyon 4. https://doi.org/10.1016/j.heliyon.2018.e00722.

Hammer, O., Harper, D.A.T., Ryan, P.D., 2001. PAST: Paleontological statistics software package for education and data analysis. Palaeontol. Electron. 4, 1–9.

Han, Y., Perner, M., 2015. The globally widespread genus *Sulfurimonas*: versatile energy metabolisms and adaptations to redox clines. Front. Microbiol. 6 https://doi.org/10.3389/fmicb.2015.00989.

Handley, K.M., VerBerkmoes, N.C., Steefel, C.I., Williams, K.H., Sharon, I., Miller, C.S., Frischkorn, K.R., Chourey, K., Thomas, B.C., Shah, M.B., Long, P.E., Hettich, R.L., Banfield, J.F., 2013. Biostimulation induces syntrophic interactions that impact C, S and N cycling in a sediment microbial community. ISME J 7, 800–816. https://doi.org/10.1038/ismej.2012.148.

Hansel, C.M., Zeiner, C.A., Santelli, C.M., Webb, S.M., 2012. Mn(II) oxidation by an ascomycete fungus is linked to superoxide production during asexual reproduction. Proc. Natl. Acad. Sci. U. S. A. 109, 12621–12625. https://doi.org/10.1073/pnas.1203885109.

Heidelberg, J.F., Seshadri, R., Haveman, S.A., Hemme, C.L., Paulsen, I.T., Kolonay, J.F., Eisen, J.A., Ward, N., Methe, B., Brinkac, L.M., Daugherty, S.C., Deboy, R.T., Dodson, R.J., Durkin, A.S., Madupu, R., Nelson, W.C., Sullivan, S.A., Fouts, D., Haft, D.H., Selengut, J., Peterson, J.D., Davidsen, T.M., Zafar, N., Zhou, L., Radune, D., Dimitrov, G., Hance, M., Tran, K., Khouri, H., Gill, J., Utterback, T.R., Feldblyum, T.V., Wall, J.D., Voordouw, G., Fraser, C.M., 2004. The genome sequence of the anaerobic, sulfate-reducing bacterium *Desulfovibrio vulgaris* Hildenborough. Nat. Biotechnol. 22, 554–559. https://doi.org/10.1038/nbt959.

Hemmat-Jou, M.H., Safari-Sinegani, A.A., Mirzaie-Asl, A., Tahmourespour, A., 2018. Analysis of microbial communities in heavy metals-contaminated soils using the metagenomic approach. Ecotoxicology 27, 1281–1291. https://doi.org/10.1007/s10646-018-1981-x.

Herlemann, D.P., Labrenz, M., Jürgens, K., Bertilsson, S., Waniek, J.J., Andersson, A.F., 2011. Transitions in bacterial communities along the 2000 km salinity gradient of the Baltic Sea. ISME J 5, 1571–1579. https://doi.org/10.1038/ismej.2011.41.

Hu, M.Z.-C., Norman, J.M., Faison, B.D., Reeves, M.E., 1996. Biosorption of uranium by *Pseudomonas aeruginosa* strain CSU: Characterization and comparison studies. Biotechnol. Bioeng. 51, 237–247. https://doi.org/10.1002/(SICI)1097-0290(19960720)51:2<237::AID-BIT14>3.0.CO;2-J.

Hua, B., Xu, H., Terry, J., Deng, B., 2006. Kinetics of uranium(VI) reduction by hydrogen sulfide in anoxic aqueous systems. Environ. Sci. Technol. 40, 4666–4671. https://doi.org/10.1021/es051804n.

Huertas, F.J., Caballero, E., Jiménez de Cisneros, C., Huertas, F., Linares, J., 2001. Kinetics of montmorillonite dissolution in granitic solutions. Appl. Geochem. 16, 397–407. https://doi.org/10.1016/S0883-2927(00)00049-4.

Huertas, F., Fariña, P., Farias, J., García-Siñeriz, J.L., Villar, M.V., Fernández, A.M., Martín, P.L., Elorza, F.J., Gens, A., Sánchez, M., Lloret, A., Samper, J., Martínez, M.Á., 2006. Full-scale Engineered Barriers Experiment. Updated Final Report 1994-2004. ENRESA Technical Report 05-0/2006.

Hugerth, L.W., Wefer, H.A., Lundin, S., Jakobsson, H.E., Lindberg, M., Rodin, S., Engstrand, L., Andersson, A.F., 2014. DegePrime, a program for degenerate primer design for broad-taxonomic-range PCR in microbial ecology studies. Appl. Environ. Microbiol. 80, 5116–5123. https://doi.org/10.1128/AEM.01403-14.

Hung, C.-H., Chang, Y.-T., Chang, Y.-J., 2011. Roles of microorganisms other than *Clostridium* and *Enterobacter* in anaerobic fermentative biohydrogen production systems – a review. Bioresour. Technol. 102, 8437–8444. https://doi.org/10.1016/j.biortech.2011.02.084.

Huy, N.D., Tien, N.T.T., Huyen, L.T., Quang, H.T., Tung, T.Q., Luong, N.N., Park, S.-M., 2017. Screening and production of manganese peroxidase from *Fusarium* sp. on residue materials. Mycobiology 45, 52–56. https://doi.org/10.5941/MYCO.2017.45.1.52.

Iskander, A.L., Khald, E.M., Sheta, A.S., 2011. Zinc and manganese sorption behavior by natural zeolite and bentonite. Ann. Agric. Sci. 56, 43–48. https://doi.org/10.1016/j.aoas.2011.05.002.

Jochum, L.M., Schreiber, L., Marshall, I.P.G., Jørgensen, B.B., Schramm, A., Kjeldsen, K. U., 2018. Single-cell genomics reveals a diverse metabolic potential of uncultivated *Desulfatiglans*-related Deltaproteobacteria widely distributed in marine sediment. Front. Microbiol. 9 https://doi.org/10.3389/fmicb.2018.02038.

Kang, T.S., Korber, D.R., Tanaka, T., 2014. Metabolic engineering of a glycerol-oxidative pathway in *Lactobacillus panis* PM1 for utilization of bioethanol thin stillage: potential to produce platform chemicals from glycerol. Appl. Environ. Microbiol. 80, 7631–7639. https://doi.org/10.1128/AEM.01454-14.

Kaufhold, S., Dohrmann, R., Gröger-Trampe, J., 2017. Reaction of native copper in contact with pyrite and bentonite in anaerobic water at elevated temperature. Corros. Eng. Sci. Technol. 52, 349–358. https://doi.org/10.1080/1478422X.2017.1292201.

Kazy, S.K., Sar, P., D'Souza, S.F., 2008. Studies on uranium removal by the extracellular polysaccharide of a *Pseudomonas aeruginosa* strain. Bioremediat. J. 12, 47–57. https://doi.org/10.1080/10889860802052870.

Kazy, S.K., D'Souza, S.F., Sar, P., 2009. Uranium and thorium sequestration by a *Pseudomonas* sp.: Mechanism and chemical characterization. J. Hazard. Mater. 163, 65–72. https://doi.org/10.1016/j.jhazmat.2008.06.076.

Khan, N.H., Bondici, V.F., Medihala, P.G., Lawrence, J.R., Wolfaardt, G.M., Warner, J., Korber, D.R., 2013. Bacterial diversity and composition of an alkaline uranium mine tailings-water interface. J. Microbiol. 51, 558–569. https://doi.org/10.1007/s12275-013-3075-z.

King, F., Hall, D.S., Keech, P.G., 2017. Nature of the near-field environment in a deep geological repository and the implications for the corrosion behaviour of the container. Corros. Eng. Sci. Technol. 52, 25–30. https://doi.org/10.1080/1478422X.2017.1330736.

Kitjanukit, S., Takamatsu, K., Okibe, N., 2019. Natural attenuation of Mn(II) in metal refinery wastewater: Microbial community structure analysis and isolation of a new Mn(II)-oxidizing bacterium *Pseudomonas* sp. SK3. Water 11, 507. https://doi.org/10.3390/w11030507.

König, H., Claus, H., Varma, A., 2010. Prokaryotic Cell Wall Compounds: Structure and Biochemistry. Springer Science & Business Media.

Kuever, J., 2014. The family desulfobacteraceae. In: Rosenberg, E., DeLong, E.F., Lory, S., Stackebrandt, E., Thompson, F. (Eds.), The Prokaryotes: Deltaproteobacteria and Epsilonproteobacteria. Springer Berlin Heidelberg, Berlin, Heidelberg, pp. 45–73. https://doi.org/10.1007/978-3-642-39044-9_266.

Kutvonen, H., Rajala, P., Carpén, L., Bomberg, M., 2015. Nitrate and ammonia as nitrogen sources for deep subsurface microorganisms. Front. Microbiol. 6 https://doi.org/10.3389/fmicb.2015.01079.

Leschine, S., Paster, B.J., 2015. Spirochaeta. In: Bergey's Manual of Systematics of Archaea and Bacteria. American Cancer Society, pp. 1–18. https://doi.org/10.1002/9781118960608.gbm01248.

Leupin, O.X., Bernier-Latmani, R., Bagnoud, A., Moors, H., Leys, N., Wouters, K., Stroes-Gascoyne, S., 2017. Fifteen years of microbiological investigation in Opalinus Clay at the Mont Terri rock laboratory (Switzerland). Swiss J. Geosci. 110, 343–354. https://doi.org/10.1007/s00015-016-0255-y.

Liu, G., Qiu, S., Liu, B., Pu, Y., Gao, Z., Wang, J., Jin, R., Zhou, J., 2017. Microbial reduction of Fe(III)-bearing clay minerals in the presence of humic acids. Sci. Rep. 7, 45354. https://doi.org/10.1038/srep45354.

Liu, W., Langenhoff, A.A.M., Sutton, N.B., Rijnaarts, H.H.M., 2018. Biological regeneration of manganese(IV) and iron(III) for anaerobic metal oxide-mediated removal of pharmaceuticals from water. Chemosphere 208, 122–130. https://doi.org/10.1016/j.chemosphere.2018.05.097.

Lopez-Fernandez, M., Cherkouk, A., Vilchez-Vargas, R., Jauregui, R., Pieper, D., Boon, N., Sanchez-Castro, I., Merroun, M.L., 2015. Bacterial diversity in bentonites, engineered barrier for deep geological disposal of radioactive wastes. Microb. Ecol. 70, 922–935. https://doi.org/10.1007/s00248-015-0630-7.

Lopez-Fernandez, M., Vilchez-Vargas, R., Jroundi, F., Boon, N., Pieper, D., Merroun, M. L., 2018. Microbial community changes induced by uranyl nitrate in bentonite clay microcosms. Appl. Clay Sci. 160, 206–216. https://doi.org/10.1016/j.clay.2017.12.034.

Lovley, D.R., Roden, E.E., Phillips, E.J.P., Woodward, J.C., 1993. Enzymatic iron and uranium reduction by sulfate-reducing bacteria. Mar. Geol. 113, 41–53. https://doi.org/10.1016/0025-3227(93)90148-O.

Luo, H., Zheng, P., Xie, F., Yang, R., Liu, L., Han, S., Zhao, Y., Bilal, M., 2019. Co-production of solvents and organic acids in butanol fermentation by *Clostridium acetobutylicum* in the presence of lignin-derived phenolics. RSC Adv. 9, 6919–6927. https://doi.org/10.1039/C9RA00325H.

Martinez, R.J., Wu, C.H., Beazley, M.J., Andersen, G.L., Conrad, M.E., Hazen, T.C., Taillefert, M., Sobecky, P.A., 2014. Microbial community responses to organophosphate substrate additions in contaminated subsurface sediments. PLoS One 9, e100383. https://doi.org/10.1371/journal.pone.0100383.

Masurat, P., Eriksson, S., Pedersen, K., 2010. Evidence of indigenous sulphate-reducing bacteria in commercial Wyoming bentonite MX-80. Appl. Clay Sci. 47, 51–57. https://doi.org/10.1016/j.clay.2008.07.002.

McMurdie, P.J., Holmes, S., 2013. phyloseq: an R package for reproducible interactive analysis and graphics of microbiome census data. PLoS One 8. https://doi.org/10.1371/journal.pone.0061217 e61217.

Merroun, M.L., Raff, J., Rossberg, A., Hennig, C., Reich, T., Selenska-Pobell, S., 2005. Complexation of uranium by cells and S-layer sheets of *Bacillus sphaericus* JG-A12. Appl. Environ. Microbiol. 71, 5532–5543. https://doi.org/10.1128/AEM.71.9.5532-5543.2005.

Missana, T., Alonso, U., Turrero, M.J., 2003. Generation and stability of bentonite colloids at the bentonite/granite interface of a deep geological radioactive waste repository. J. Contam. Hydrol. 61, 17–31. https://doi.org/10.1016/S0169-7722(02)00110-9.

Morales, M., Cano, M., Merroun, M.L., Martín, I., 2019. *Potencial de Hongos Aislados de Bentonitas en el Biorremedio de Selenio y Teluro* [Conference abstract]. XXVII Congreso Nacional de Microbiología, Málaga, Spain, 2-5 July.

Nessa, S., Idemitsu, K., Yamasaki, Y., Inagaki, Y., Arima, T., 2007. Measurement of pH of the Compacted Bentonite Under the Reducing Condition, 67. Memoirs of the Faculty of Engineering, Kyushu University, pp. 25–31.

Newsome, L., Morris, K., Lloyd, J.R., 2014a. The biogeochemistry and bioremediation of uranium and other priority radionuclides. Chem. Geol. 363, 164–184. https://doi.org/10.1016/j.chemgeo.2013.10.034.

Newsome, L., Morris, K., Trivedi, D., Atherton, N., Lloyd, J.R., 2014b. Microbial reduction of uranium(VI) in sediments of different lithologies collected from Sellafield. Appl. Geochem. 51, 55–64. https://doi.org/10.1016/j.apgeochem.2014.09.008.

Newsome, L., Morris, K., Shaw, S., Trivedi, D., Lloyd, J.R., 2015. The stability of microbially reduced U(IV); impact of residual electron donor and sediment ageing. Chem. Geol. 409, 125–135. https://doi.org/10.1016/j.chemgeo.2015.05.016.

Overton, B.E., Stewart, E.L., Wenner, N.G., 2006. Manganese oxidation in Petri disease fungi as a novel taxonomic character. Phytopathol. Mediterr. 45, S131–S134.

Patil, Y., Junghare, M., Müller, N., 2016. Fermentation of glycerol by *Anaerobium acetethylicum* and its potential use in biofuel production. Microb. Biotechnol. 10, 203–217. https://doi.org/10.1111/1751-7915.12484.

Payer, J.H., Finsterle, S., Apps, J.A., Muller, R.A., 2019. Corrosion performance of engineered barrier system in deep horizontal drillholes. Energies 12, 1491. https://doi.org/10.3390/en12081491.

Payne, R.B., Gentry, D.M., Rapp-Giles, B.J., Casalot, L., Wall, J.D., 2002. Uranium reduction by *Desulfovibrio desulfuricans* strain G20 and a cytochrome c3 mutant. Appl. Environ. Microbiol. 68, 3129–3132. https://doi.org/10.1128/AEM.68.6.3129-3132.2002.

Pedersen, K., Bengtsson, A., Blom, A., Johansson, L., Taborowski, T., 2017. Mobility and reactivity of sulphide in bentonite clays – Implications for engineered bentonite barriers in geological repositories for radioactive wastes. Appl. Clay Sci. 146, 495–502. https://doi.org/10.1016/j.clay.2017.07.003.

Pentráková, L., Su, K., Pentrák, M., Stucki, J.W., 2013. A review of microbial redox interactions with structural Fe in clay minerals. Clay Miner. 48, 543–560. https://doi.org/10.1180/claymin.2013.048.3.10.

Perdrial, J.N., Warr, L.N., Perdrial, N., Lett, M.-C., Elsass, F., 2009. Interaction between smectite and bacteria: Implications for bentonite as backfill material in the disposal of nuclear waste. Chem. Geol. 264, 281–294. https://doi.org/10.1016/j.chemgeo.2009.03.012.

Petrie, L., North, N.N., Dollhopf, S.L., Balkwill, D.L., Kostka, J.E., 2003. Enumeration and characterization of iron(III)-reducing microbial communities from acidic subsurface sediments contaminated with uranium(VI). Appl. Environ. Microbiol. 69, 7467–7479. https://doi.org/10.1128/aem.69.12.7467-7479.2003.

Povedano-Priego, C., Jroundi, F., Lopez-Fernandez, M., Sánchez-Castro, I., Martin-Sánchez, I., Huertas, F.J., Merroun, M.L., 2019. Shifts in bentonite bacterial community and mineralogy in response to uranium and glycerol-2-phosphate exposure. Sci. Total Environ. 692, 219–232. https://doi.org/10.1016/j.scitotenv.2019.07.228.

Povedano-Priego, C., Jroundi, F., Lopez-Fernandez, M., Shrestha, R., Spanek, R., Martín-Sánchez, I., Villar, M.V., Ševců, A., Dopson, M., Merroun, M.L., 2021. Deciphering indigenous bacteria in compacted bentonite through a novel and efficient DNA extraction method: Insights into biogeochemical processes within the Deep Geological Disposal of nuclear waste concept. J. Hazard. Mater. 408, 124600. https://doi.org/10.1016/j.jhazmat.2020.124600.

Qatibi, A.I., Bennisse, R., Jana, M., Garcia, J.-L., 1998. Anaerobic degradation of glycerol by *Desulfovibrio fructosovorans* and *D. carbinolicus* and evidence for glycerol-dependent utilization of 1,2-propanediol. Curr. Microbiol. 36, 283–290.

Quast, C., Pruesse, E., Yilmaz, P., Gerken, J., Schweer, T., Yarza, P., Peplies, J., Glöckner, F.O., 2013. The SILVA ribosomal RNA gene database project: improved data processing and web-based tools. Nucleic Acids Res. 41, D590–D596. https://doi.org/10.1093/nar/gks1219.

Rajala, P., Carpén, L., Vepsäläinen, M., Raulio, M., Sohlberg, E., Bomberg, M., 2015. Microbially induced corrosion of carbon steel in deep groundwater environment. Front. Microbiol. 6. https://doi.org/10.3389/fmicb.2015.00647.

Ren, Y., Bao, H., Wu, Q., Wang, H., Gai, T., Shao, L., Wang, S., Tang, H., Li, Y., Wang, X., 2020. The physical chemistry of uranium(VI) immobilization on manganese oxides. J. Hazard. Mater. 391, 122207. https://doi.org/10.1016/j.jhazmat.2020.122207.

Robertson, C.E., Harris, J.K., Wagner, B.D., Granger, D., Browne, K., Tatem, B., Feazel, L. M., Park, K., Pace, N.R., Frank, D.N., 2013. Explicet: graphical user interface software for metadata-driven management, analysis and visualization of microbiome data. Bioinformatics 29, 3100–3101. https://doi.org/10.1093/bioinformatics/btt526.

Rozalen, M.L., Huertas, F.J., Brady, P.V., Garcia-Palma, S.T., Linares, J., 2008. Experimental study of the effect of pH on the kinetics of montmorillonite dissolution at 25°C. Geochim. Comochim. Acta 72, 4224–4253.

Saad, S., Bhatnagar, S., Tegetmeyer, H.E., Geelhoed, J.S., Strous, M., Ruff, S.E., 2017. Transient exposure to oxygen or nitrate reveals ecophysiology of fermentative and sulfate-reducing benthic microbial populations. Environ. Microbiol. 19, 4866–4881. https://doi.org/10.1111/1462-2920.13895.

Safonov, A.V., Babich, T.L., Sokolova, D.S., Grouzdev, D.S., Tourova, T.P., Poltaraus, A. B., Zakharova, E.V., Merkel, A.Y., Novikov, A.P., Nazina, T.N., 2018. Microbial community and in situ bioremediation of groundwater by nitrate removal in the zone of a radioactive waste surface repository. Front. Microbiol. 9 https://doi.org/10.3389/fmicb.2018.01985.

Salome, K.R., Green, S.J., Beazley, M.J., Webb, S.M., Kostka, J.E., Taillefert, M., 2013. The role of anaerobic respiration in the immobilization of uranium through biomineralization of phosphate minerals. Geochim. Cosmochim. Acta 106, 344–363. https://doi.org/10.1016/j.gca.2012.12.037.

Santelli, C.M., Webb, S.M., Dohnalkova, A.C., Hansel, C.M., 2011. Diversity of Mn oxides produced by Mn(II)-oxidizing fungi. Geochim. Cosmochim. Acta 75, 2762–2776. https://doi.org/10.1016/j.gca.2011.02.022.

Segata, N., Waldron, L., Ballarini, A., Narasimhan, V., Jousson, O., Huttenhower, C., 2012. Metagenomic microbial community profiling using unique clade-specific marker genes. Nat. Methods 9, 811–814. https://doi.org/10.1038/nmeth.2066.

Smart, N.R., Reddy, B., Rance, A.P., Nixon, D.J., Frutschi, M., Bernier-Latmani, R., Diomidis, N., 2017. The anaerobic corrosion of carbon steel in compacted bentonite exposed to natural Opalinus Clay porewater containing native microbial populations. Corros. Eng. Sci. Technol. 52, 101–112. https://doi.org/10.1080/1478422X.2017.1315233.

Soo Lee, S., Li, W., Kim, C., Cho, M., Catalano, G.J., Lafferty, B.J., Decuzzi, P., Fortner, J. D., 2015. Engineered manganese oxide nanocrystals for enhanced uranyl sorption and separation. Environ. Sci. Nano 2, 500–508. https://doi.org/10.1039/C5EN00010F.

Stone, W., Kroukamp, O., Moes, A., McKelvie, J., Korber, D.R., Wolfaardt, G.M., 2016. Measuring microbial metabolism in atypical environments: Bentonite in used nuclear fuel storage. J. Microbiol. Methods 120, 79–90. https://doi.org/10.1016/j.mimet.2015.11.006.

Stroes-Gascoyne, S., Hamon, C.J., Maak, P., Russell, S., 2010. The effects of the physical properties of highly compacted smectitic clay (bentonite) on the culturability of indigenous microorganisms. Appl. Clay Sci. 47, 155–162. https://doi.org/10.1016/j.clay.2008.06.010.

Stylo, M., Neubert, N., Roebbert, Y., Weyer, S., Bernier-Latmani, R., 2015. Mechanism of uranium reduction and immobilization in *Desulfovibrio vulgaris* biofilms. Environ. Sci. Technol. 49, 10553–10561. https://doi.org/10.1021/acs.est.5b01769.

Sun, H., Yang, Q., Peng, Y., Shi, X., Wang, S., Zhang, S., 2009. Nitrite accumulation during the denitrification process in SBR for the treatment of pre-treated landfill leachate. Chin. J. Chem. Eng. 17, 1027–1031. https://doi.org/10.1016/S1004-9541(08)60312-2.

Svensson, D., Dueck, A., Nilsson, U., Olsson, S., Sandén, T., Lydmark, S., Jägerwall, S., Pedersen, K., Hansen, S., 2011. Alternative buffer material – Status of the ongoing laboratory investigation of reference materials and test package 1. In: SKB Technical Report. Swedish Nuclear Fuel & Waste Management Co, pp. 1–146.

Takai, K., Suzuki, M., Nakagawa, S., Miyazaki, M., Suzuki, Y., Inagaki, F., Horikoshi, K., 2006. *Sulfurimonas paralvinellae* sp. nov., a novel mesophilic, hydrogen- and sulfur-oxidizing chemolithoautotroph within the Epsilonproteobacteria isolated from a deep-sea hydrothermal vent polychaete nest, reclassification of *Thiomicrospira denitrificans* as *Sulfurimonas denitrificans* comb. nov. and emended description of the genus *Sulfurimonas*. Int. J. Syst. Evol. Microbiol. 56, 1725–1733. https://doi.org/10.1099/ijs.0.64255-0.

Temudo, M.F., Poldermans, R., Kleerebezem, R., van Loosdrecht, M.C.M., 2008. Glycerol fermentation by (open) mixed cultures: a chemostat study. Biotechnol. Bioeng. 100, 1088–1098. https://doi.org/10.1002/bit.21857.

Vecchia, E.D., Veeramani, H., Suvorova, E.I., Wigginton, N.S., Bargar, J.R., Bernier-Latmani, R., 2010. U(VI) reduction by spores of *Clostridium acetobutylicum*. Res. Microbiol. 161, 765–771. https://doi.org/10.1016/j.resmic.2010.08.001.

Villar, M.V., Pérez Del Villar, L., Martín, P.L., Pelayo, M., Fernández, A.M., Garralón, A., Cuevas, J., Leguey, S., Caballero, E., Huertas, F.J., others, 2006. The study of Spanish clays for their use as sealing materials in nuclear waste repositories: 20 years of progress. J. Iber. Geol. 32, 15–36.

Warnes, G.R., Bolker, B., Bonebakker, L., Gentleman, R., Liaw, W.H.A., Lumley, T., Maechler, M., Magnusson, A., Moeller, S., Schwartz, M., Venables, B., 2019. gplots: Various R Programming Tools for Plotting Data.

Warr, L.N., 2021. IMA–CNMNC approved mineral symbols. Mineral. Mag. 85, 291–320.

Weidenmaier, C., Peschel, A., 2008. Teichoic acids and related cell-wall glycopolymers in Gram-positive physiology and host interactions. Nat. Rev. Microbiol. 6, 276–287. https://doi.org/10.1038/nrmicro1861.

Wu, W.-M., Carley, J., Green, S.J., Luo, J., Kelly, S.D., Nostrand, J.V., Lowe, K., Mehlhorn, T., Carroll, S., Boonchayanant, B., Löffler, F.E., Watson, D., Kemner, K.M., Zhou, J., Kitanidis, P.K., Kostka, J.E., Jardine, P.M., Criddle, C.S., 2010. Effects of nitrate on the stability of uranium in a bioreduced region of the subsurface. Environ. Sci. Technol. 44, 5104–5111. https://doi.org/10.1021/es1000837.

Xie, X., Müller, N., 2018. Enzymes involved in the anaerobic degradation of phenol by the sulfate-reducing bacterium *Desulfatiglans anilini*. BMC Microbiol. 18, 93. https://doi.org/10.1186/s12866-018-1238-0.

Xu, J., Veeramani, H., Qafoku, N.P., Singh, G., Riquelme, M.V., Pruden, A., Kukkadapu, R.K., Gartman, B.N., Hochella, M.F., 2017. Efficacy of acetate-amended biostimulation for uranium sequestration: combined analysis of sediment/groundwater geochemistry and bacterial community structure. Appl. Geochem. 78, 172–185. https://doi.org/10.1016/j.apgeochem.2016.12.024.

Yilmaz, P., Yarza, P., Rapp, J.Z., Glöckner, F.O., 2016. Expanding the world of marine bacterial and archaeal clades. Front. Microbiol. 6 https://doi.org/10.3389/fmicb.2015.01524.

Youssef, N.H., Elshahed, M.S., 2014. The phylum planctomycetes. In: Rosenberg, E., DeLong, E.F., Lory, S., Stackebrandt, E., Thompson, F. (Eds.), The Prokaryotes: Other Major Lineages of Bacteria and the Archaea. Springer Berlin Heidelberg, Berlin, Heidelberg, pp. 759–810. https://doi.org/10.1007/978-3-642-38954-2_155.